CHALMERS
UNIVERSITY OF TECHNOLOGY

Prediction of Lateral Instability and Reducing Rearward Amplification of Autonomous Long Combination Vehicles

Master's thesis in Complex Adaptive Systems

Henrik Esmaili

Department of Mechanics and Maritime Sciences
CHALMERS UNIVERSITY OF TECHNOLOGY
Gothenburg, Sweden 2020

Master's thesis 2020:09

Prediction of Lateral Instability and Reducing Rearward Amplification of Autonomous Long Combination Vehicles

Henrik Esmaili

CHALMERS
UNIVERSITY OF TECHNOLOGY

Department of Mechanics and Maritime Sciences
Vehicle Dynamics Group
Chalmers University of Technology
Gothenburg, Sweden 2020

Prediction of Lateral Instability and Reducing Rearward Amplification
of Autonomous Long Combination Vehicles
Henrik Esmaili

Academical Supervisor: Leon Henderson, Volvo Group Trucks Technology, Chalmers University of Technology
Industrial Supervisor: Yangyan Gao, Volvo Group Trucks Technology
Examiner: Bengt Jacobsson, Chalmers University of Technology

Master's Thesis 2020:09
Department of Mechanics and Maritime Sciences
Vehicle Dynamics Group
Chalmers University of Technology
SE-412 96 Gothenburg
Telephone +46 31 772 1000

Cover: Visualisation of a truck experiencing lateral instability. Created with Volvo GTT VTMs animation environment.

Typeset in LaTeX
Gothenburg, Sweden 2020

Prediction of Lateral Instability and Reducing Rearward Amplification
of Autonomous Long Combination Vehicles
Henrik Esmaili
Department of Mechanics and Maritime Sciences
Chalmers University of Technology

Abstract

Autonomously driven long combination vehicles have potential advantages such as higher levels of safety, greater fuel efficiency and reduced total cost of ownership per ton of unit freight. On the other hand, long combination vehicles are more prone to lateral instability such as trailer swinging. In addition, lateral instability is far more difficult to control compared to shorter combinations. This thesis presents an intuitive and simple controller, designed for an autonomous highway driving A-double. The controller is developed to both reduce lateral instability and the rearward amplification that a vehicle generates during a typical highway lane change and step-steer manouvre. A linear single-track model of an A-double was employed as a foundation for the controller. The linear single-track model was verified against a simulation model and data from real testing of an A-double. The performance of the controller was tested for different manoeuvres as well as compared against the uncontrolled case, a band-stop filter and a low-pass filter. The results showed that the controller reduced rearward amplification for all manoeuvres. However, open-loop and closed-loop testing of the controller in simulation is necessary before any real testing is conducted.

Keywords: Long combination vehicles, Autonomous driving, Lateral instability, Rearward amplification, Control method

Acknowledgements

I would like to take the opportunity to thank a couple of individuals. Firstly, I would like to thank my supervisors Leon Henderson and Yangyan Gao for their constant support and priceless discussions throughout the project. This thesis would not be what it is without your help. Secondly, I would like to thank my examiner Professor Bengt Jacobsson for his valuable guidance and words of advice, but most importantly for taking on the project along with me. In addition, I adress a big thank you to Professor Timothy Gordon and Shammi Rahman for their engagement in this thesis and providing me with helpful insight.

This thesis is not the sole work of a single person. Without the following contributions the thesis would not be possible: Professor Timothy Gordon who lent out his A-double solver, Niklas Fröjd who helped me to obtain the test data and Trafikverket who shared the test data of the A-double. I am truly grateful for your help.

To all my friends and family, I am very thankful for your support during these past 20 weeks. It has been a roller coaster ride and I am lucky to have had all of you by my side.

Last but not least, I would like to thank the Volvo Group Truck Technology for the opportunity to do this master thesis thesis with you and by doing that, helping me fulfil my long dream of working with vehicles. I will cherish this experience for a long time. It has been educational and has helped preparing me for a future within the industry.

Henrik Esmaili, Gothenburg, April 2020

Contents

Abbreviations

ASIL Automotive Safety Integrity Level.

DAE Differential Algebraic Equation.
DLC Double Lane Change.

GFG Global Force Generator.

LCV Long Combination Vehicle.
LQR Linear Quadratic Regulator.
LTI Linear time-invariant.

MPC Model Predictive Control.

ODE Ordinary Differential Equation.

PP Preview Points.
PT Preview Time.

RWA Rearward Amplification.

SLC Single Lane Change.
SS Step-Steer.

TSM Traffic Situation Manager.

VMM Vehicle Motion Manager.

1
Introduction

1.1 Background

One of the current trends in the automotive industry is towards highway automation. With potential advantages such as higher safety and greater fuel efficiency [1], the truck industry has started developing self-driving vehicles. A paper by Toheed Ghandriz [2] showed that replacing the driver of a conventional heavy vehicle with an automated driving system, leading to the total ownership cost per ton of unit freight could be significantly reduced. Furthermore, it was also shown that by using long heavy vehicle combinations, such as A-doubles, the fuel consumption per ton of goods transported was reduced compared to smaller combinations. As a side-effect besides lowered fuel cost, the environment benefits from the lowered fuel consumption. Therefore, combining autonomous driving systems with long heavy vehicle combinations could generate more profit for logistic companies. Volvo Group, one of the global truck manufacturers, has shown great interest in this technology-intensive arena.

It may take some time before fully autonomous trucks will be deployed on public roads in all driving scenarios. One of the reasons is the high requirements on safety standards described by ISO26262 [3], which has been created to improve vehicle safety. Automotive Safety Integrity Level (ASIL) values are related to hazards analysis in the automotive systems with ASIL-D being the highest rating, which means the hazards are common, high severity and difficult to control [4]. For long combination vehicles the lateral instability is far more difficult to control compared to shorter combinations. This report will focus on developing a system for autonomous driving long combination vehicles (LCVs) to ensure that the vehicle dynamics remains within a "safe zone" where lateral instability will not occur.

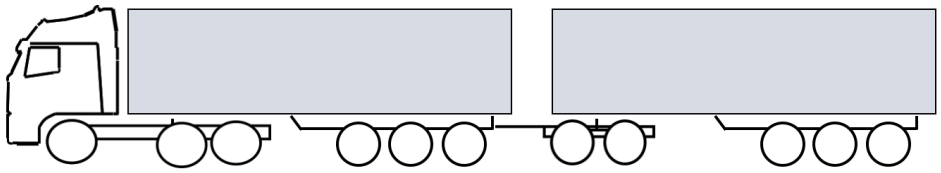

Figure 1.1: A simple drawing of an A-double. Starting from the left: The first unit is the tractor and the second is the first semitrailer. The third is the dolly and the fourth is the second semitrailer. The A-double typically has 11 axles, whereof the first axle on the tractor is the only steerable.

Long combination vehicles have shown promise for transporting goods due to better efficiency, fuel saving and carrying capacity [5] as opposed to conventional truck configurations. Figure 1.1 shows an A-double, which is a type of LCV. Long combination vehicles are combinations of a series of trailers connected to tractor trucks; much like how a cargo train works. Although uncommon in Europe, LCVs are common in countries such as USA and Australia [6]. However, using LCVs can impose increased risks relating to their multiple articulation points, such as trailer roll-over, jack-knifing and trailer-swinging [7]. One of the key measurements for instability of LCVs is rearward amplification (RWA), which is defined as the ratio of the largest observed lateral acceleration of the last trailer and the tractor. Large RWA problems tend to occur when the truck is excited at certain frequencies [8]. Therefore, those resonant frequencies should be avoided. When a skilled human driver is operating a LCV, he or she will try to avoid exciting these resonances by limiting the types of steering inputs. Similar considerations need to be made by an autonomous driving system. If not, it could lead to instability problems and in the worst case scenario, a rollover. Avoiding the undesirable excitations (steering inputs) can be more affective than reacting on a large RWA situation. Control systems that can prevent reaching the undesirable resonances is one way of creating a safety net for better lateral performance of LCVs.

1.2 Project description

1.2.1 Aim

The aim of this thesis work is to understand the lateral instability problems of highly automated LCVs and using the obtained knowledge to create a preventive steering controller to try to reduce generated RWA. This will be done by

- Understanding the instability problems of highly automated LCVs,
- Understanding how an automated driver system works,
- Proposing a verified simple vehicle model that captures the vehicle dynamics associated with rearward amplification,
- Identifying driving scenarios with large RWA values,
- Designing and verifying (by simulations) a control method which prevents large RWA values occurring and compare against two traditional frequency based filters that could alternately be used to reduce RWA.

1.2.2 Limitations

Due to the size of the topic, the following limitations will be made:

- The stability analysis will be based on linear models.
- The model is simplified to consider planar motion of the vehicle; out of plane motion, such as pitch and roll dynamics, are not included.
- The model is only valid for flat roads.
- Only yaw-motion related instability is considered. Roll-over dynamics are not included, but can be predicted if the mass properties of the trailers are known.
- Only highway driving scenarios with constant speeds will be considered.
- A linear tyre model will be used.
- Due to the availability of the test vehicle and track, vehicle testing will only be used to validate the correctness of the vehicle models. The control methods will be assessed using simulation.

1.3 Outline of thesis

More specifically, the thesis will address the following questions:

- Is it possible to use a linear single track model as a foundation for a controller designed to handle highway scenarios?
- Does the proposed control method reduce RWA for all predefined highway driving scenarios to an acceptable level?
- Does the proposed method perform better than a simple notch or low-pass filter?
- Can the results of an A-double linear single-track model represent simulation or real-world testing?

2
Vehicle Modelling

A single-track model is a simplified mathematical model intended to capture certain behaviours of a chosen vehicle type, as in the case of LCVs: yaw-rate instability which is the reason behind undesirable trailer swing. Mathematical analysis can then be conducted to find the underlying reasons for the behaviours, such as eigenfrequency analysis. Lagrangian mechanics is used in this thesis to derive the equations describing the model. The following chapter treats Lagrangian mechanics and the assumptions made for each vehicle model to derive the set of equations.

2.1 Literature review

Vehicle dynamics modelling is typically split into two different fields. Modelling of the vehicle itself and modelling of the tyres, both equivalently important since they interact with each other.

When modelling a vehicle in planar motion, one can either choose to keep the wheels on each axle separated, called a two-track model, or lump them together into one wheel in the middle of the axle, called a single-track model. Using the two-track model helps preserving more of the behaviour of the vehicle, but leads to complex equations and an increased number of terms in them. In contrast, the single-track model offers an easier way to model the vehicle but at the loss of capturing certain dynamics e.g. lateral load transfer [9]. Since the number of equations and the complexity of them increase with the number of units, the single-track model is more suitable for longer articulated vehicle combinations. This is shown by the amount of papers deriving single track models for different vehicle models [10] [11] [12]. There are exceptions, such as Chen and Taomizuka, who created a double-track model of an articulated heavy vehicle [11]. Although a single-unit model is relatively easy to derive, the complexity and difficulty rapidly increases when more units are added. To reduce the complexity, various assumptions are used when deriving the model. Leven et al [12] derived a single-track model of a truck-dolly-semitrailer combination. Peter Nilsson and Kristoffer Tagesson derived a single-track model of an A-double [13], an even more complex model than the truck-dolly-semitrailer.

The simplest tyre model is the linear tyre model. Assuming that the lateral force of the tire increases linearly with slip angle within a certain region. The coefficient used is a value that is estimated from testing but may be varied for the same vehicle given different road surfaces.There also exist more advanced tyre models. One of the

popular models is Hans B Pacejkas "Magic formula" [14]. The formula uses a range of different parameters to estimate a curve which can be used to compute the tyre force (both longitudinal and lateral) based on the combined longitudinal and lateral slip of the wheel. The name is chosen because, there is no particular physical basis for the structure of the equations chosen, but instead from mathematical estimation to capture the behaviour of the tyres. Another semi-physical based tyre model is the "TMeasy" model [15]. It uses less parameters than the magic formula and is more convenient to interpret, hence easier to use. However, TMeasy is not as accurate which does not make it suitable for situations where high-accuracy estimations are needed [16]. Another approach to model the tyre is based on physical modelling the characteristics of the tyre, such as brush model. The brush model views the tyre as an object consisting of small contact patches, that touch the ground instead of a single object making total contact. One of these models is the LuGre-model. According to its authors, it is especially suitable for feedback control since it captures the fundamental friction related behaviour [17].

2.2 Lagrangian mechanics

Lagrangian mechanics is a different way to generate the equations of motion of a mechanical system rather than the usual Newtonian approach [18]. The primary benefit of using Lagrangian mechanics is that it results in a derived system of ODEs rather than differential algebraic equations (DAEs) like Newtonian mechanics [19], but at the cost of more complex derivations to obtain the equations of motion. At a first glance it seems as a big drawback, but using symbol solving software like Mathematica or Matlab reduces the inconvenience.

The Lagrangian L is defined as

$$L = T - V, \tag{2.1}$$

where T is the kinematic energy of the system and V is the potential energy. The equation for a generalised coordinate q_i is obtained from

$$\begin{aligned} \frac{\mathrm{d}}{\mathrm{d}t}\left(\frac{\partial L}{\partial \dot{q}_i}\right) - \frac{\partial L}{\partial q_i} &= Q_i \\ Q_i &= \sum_{k=1}^{N} \mathbf{F}_k \cdot \frac{\partial \mathbf{r}_k}{\partial q_i}, \end{aligned} \tag{2.2}$$

where $\mathbf{r}_k$ is the position vector to the force $\mathbf{F}_k$. Moreover, the total virtual power on a system can be written as

$$P = Q_1\dot{q}_1 + Q_2\dot{q}_2 + ... + Q_m\dot{q}_m = \sum_{i=1}^{m} Q_i \cdot \dot{q}_i, \tag{2.3}$$

where $\dot{q}_i$ is the time derivative of generalised coordinate q_i. From solving the equations above, one can derive a set of equations describing the system. By rearranging

the terms and linearizing each equation one obtains the following ODE-equation system variables gives

$$M\vec{\ddot{q}} + K\vec{\dot{q}} + H\vec{q} + L = 0, \tag{2.4}$$

which is much easier to solve and conduct analysis on compared to a non-linear system. To further simplify the system, it is rewritten to the first-order differential equation system

$$\vec{\dot{x}} = A\vec{x} + B\vec{u}, \tag{2.5}$$

where $\vec{u}$ is the input vector.

2.3 Derivation of tractor and semitrailer single-track vehicle model

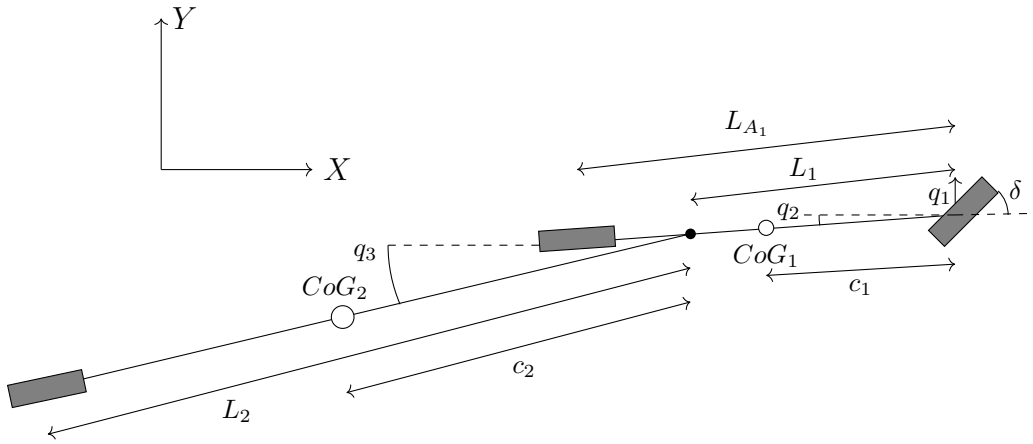

Figure 2.1: Single-track model of a tractor-semitrailer.

Figure 2.1 shows the tractor-semitrailer model. The semitrailer is attached to the fifth wheel in front of the rear axle of the tractor. In this model, the tandem rear axle on the tractor is grouped into one axle. Moreover, angles are assumed to be small and linear tyre models are used. In this model the generalised coordinates are

$$\vec{q} = [Y_1, \phi_1, \phi_2]^T = [q_1, q_2, q_3]^T, \tag{2.6}$$

where Y_1 is the position of the front axle in the tractor in Y-axis, ϕ_1 is the yaw angle for the tractor and ϕ_2 is the yaw angle for the trailer. From these assumptions a linearized model is derived. This model will not be used in this thesis but the derivations for the tractor and semitrailer model are presented in Appendix A.1 as a demonstration of how to derive a linear single-track tractor-semitrailer vehicle model.

2.4 Derivation of A-double combination single-track vehicle model

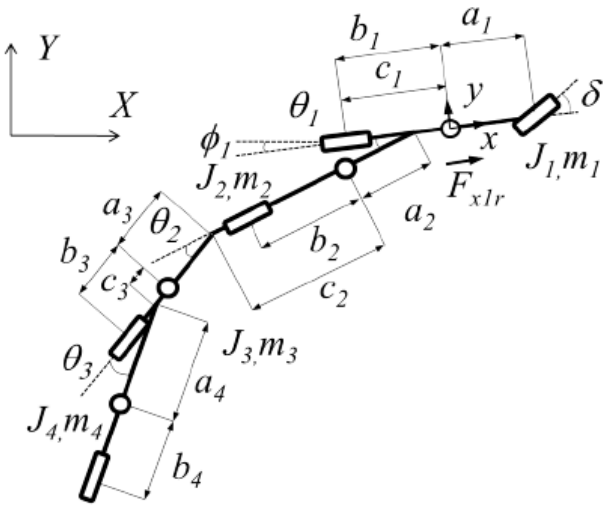

Figure 2.2: A single-track model of an A-double with five axles. Permission to be used by Peter Nilsson [13].

The difference between an A-double and a tractor-semitrailer combination is that an additional dolly-semitrailer is attached to the rear of the first semitrailer. Figure 2.2 presents an example of a single-track model of an A-double with five axles. This model is not going to be used in this thesis work and is just shown as a visual example of an A-double combination single-track model. Instead, an A-double combination single-track model including all 11 axles is going to be deployed. As in section 2.3, the approach to obtain the equations is Lagrangian mechanics. However, since the number of expressions and variables increase, so does the complexity of the equations. To spare the unnecessary time deriving the equations, a solver provided by Professor Timothy Gordon at Lincoln University[1] will be used to generate equations of an A-double.

[1]Professor Timothy Gordon, University of Lincoln, `https://staff.lincoln.ac.uk/876222e4-9b1d-46a3-803b-0f115ce2d3e6`

2.5 Tyre model

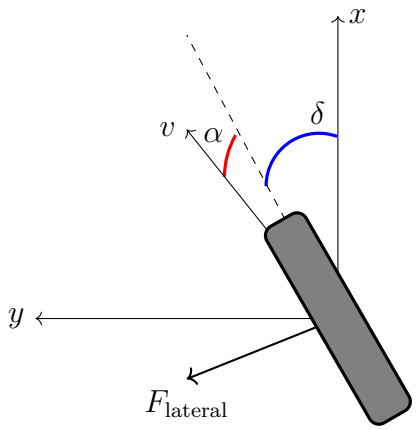

Figure 2.3: Simple representation of the forces and velocities acting on a tyre (only lateral force shown).

A tyre model represents the forces generated on the tyres when driving. The simplest of the model is the linearized tyre model. The model is defined as

$$F_{\text{lateral}} = -C \cdot \alpha, \tag{2.7}$$

where C is the cornering stiffness for the wheel and α is the slip angle for the wheel. The cornering stiffness is a constant value, determined by experiments on a specific road surface. The slip angle for a wheel is defined as

$$\alpha = -\arctan\left(\frac{v_y}{v_x}\right) + \delta \tag{2.8}$$

where v_y and v_x are the lateral and longitudinal wheel station speed at the vehicle body coordinate system in figure 2.3. δ is the angle the wheel is turned. Assuming angles are small, α can be approximated to

$$\alpha \approx -\frac{v_y}{v_x} + \delta. \tag{2.9}$$

The benefit of using a linearized tyre model is that, unlike the magic formula, it uses one parameter and still keeps the single-track model linear. An effect of keeping both the single-track and the tyre model linear is that calculating the system response becomes much simpler. For example, the eigenvalues of the system are possible to obtain.

3
Performance Metrics

By using linear ODE-systems of the vehicle models, a wide range of different tools are available to use for examining the characteristics and behaviours displayed. Furthermore, metrics to measure performance are needed for validation of the controller and linear single-track model. In this chapter, the tools and metrics used in this thesis are described and explained.

3.1 Rearward amplification

Rearward amplification ratio is defined as

$$\text{RWA} \equiv \frac{|L_{a_{\max}}|}{|F_{a_{\max}}|}, \tag{3.1}$$

where $L_{a_{\max}}$ is the largest lateral acceleration observed for the last unit. Likewise, $F_{a_{\max}}$ is the largest lateral acceleration observed for the tractor [8]. Although the value do not directly tell an exact risk of an accident happening, it gives a value that is comparable. This is useful when comparing stability against other vehicle combinations as well as when grading RWA reducing methods. A RWA value close to one is desired since it means that the last unit does not exceed that of the tractor, and as a result, the risk of lateral instability related accidents (such as roll over) is lowered.

3.2 Damping ratio

Let $\lambda_n \in \mathbb{C}$ be the n^{th} eigenvalue obtained from the matrix A. The natural frequency ω_n can be calculated by the euclidean norm

$$\omega_n = \sqrt{\lambda_n \lambda_n^*} = \|\lambda_n\|_2 \,, \tag{3.2}$$

where λ_n^* is the complex conjugate of λ_n. By taking the real part of λ_n one can obtain the damping ratio ζ_n from

$$\zeta_n = -\frac{\text{Re}(\lambda_n)}{\omega_n}. \tag{3.3}$$

Eigenvalues with the value zero indicate rigid motion, therefore no damping as such. From stability theory [20] the value ζ_n can be categorised into four distinct cases

$$\begin{aligned} \zeta &= 0 \implies \text{undamped} \\ 0 < \zeta &< 1 \implies \text{underdamped} \\ \zeta &= 1 \implies \text{critically damped} \\ \zeta &> 1 \implies \text{overdamped} \end{aligned} \tag{3.4}$$

3.3 Magnitude square coherence

Magnitude square coherence shows the correlation between the two signals a and b for a certain frequency f. It is defined as

$$Z_{ab}(f) = \frac{|G_{ab}(f)|^2}{G_{aa}(f)G_{bb}(f)} \tag{3.5}$$

where $G_{ab}(f)$ is the cross-spectral density between signals. The correlation $Z_{xy}(f)$ returns a value between zero and one, where 0 indicates no correlation between the signals and 1 the opposite [21].

3.4 Bode plot

A convenient way to examine the characteristics of a linear time-invariant (LTI) system is to take the Laplace transform of it and investigate its transfer function. The transfer function $H(s)$ is the Laplace transform of the system and is defined as

$$H(s) = \frac{Y(s)}{X(s)}, \tag{3.6}$$

where s is the frequency, $Y(s)$ and $X(s)$ are the Laplace transform of the output and input of the system. One of the common ways to view the transfer functions characteristics is through the systems frequency response. This is done by Bode plots which consists of two different plots: One is of the gain of the system on the y-axis given as a function of frequency. The second is the phase given as a function of the frequency. To ease analysis of the graphs, the gain is shown in decibel and the frequency-axis shown in semi-log values [22].

Bode plots are very useful tools when trying to find undamped resonant frequencies by observation as well as for determining how much damping is present for the specific modes. For example, a peak in the magnitude plot with a value greater than one, indicates that at that frequency the system's output will be larger than the input. In the case of yaw-rate gain to the last trailer, this can indicate that if excited at this frequency the last trailer will oscillate with a high yaw-rate leading to large RWA value. Bode plots are used in section 4.6 to analyze results from the pseudo-random steering.

4
Model Verification

Even though a linear single-track model can display certain vehicle characteristics, it still has to be tested against real test data or simulation results from a high fidelity vehicle model to verify that the single-track vehicle model can capture the motion of interest. In this chapter, the linear single-track model is compared against data from both real testing and the simulations including four different highway manoeuvres. In addition, a psuedo-random steering manoeuvre is performed to enable frequency analysis of the vehicle and create Bode plot of the models.

4.1 Verifying A-double model

Simulations using Volvo's Virtual Transport Model library (VTM), which is an in-house developed high-fidelity vehicle dynamics model are done. To verify the linear single-track model of the A-double, and the VTM model, fullstop testing on different highway-driving related manoeuvres are conducted to see the yaw-rates generated from the manoeuvre. This has been executed using steering angles for four manoeuvres as inputs to the simulation models, recorded from real testing done on an A-double (figure 1.1). The linear single-track model and VTM-model will have the same weights, number of axles, dimensions and parameters as the A-double used for testing. Moreover, the single-track model and the VTM are also compared against real test data.

The motivation behind comparing the VTM and the real test data is due to the limitations of the thesis. Since real testing of the preventive controller won't be possible, it would be preferable if the testing is done on a VTM model. Thus, it is important to know how much the VTM differs from a real A-double. The linear single-track model and the VTM environment were given the same parameters, speed and steering angles as the real test data. This is true for all the following figures for the linear single-track model. From now on the tractor is referred to as the Hunter, the first semitrailer as Target 1 and the last semitrailer as Target 2. Data for the dolly is not presented due to the lack of instrumentation on the dolly used for the real world experiments.

4.2 Single lane change manoeuvre

The single lane change can be viewed as a single sinusoidal steering angle input. It can be viewed from the driver's perspective as changing from one driving lane to an adjacent one. Figure 4.1 displays the steering angles used to perform the manoeuvre by the driver.

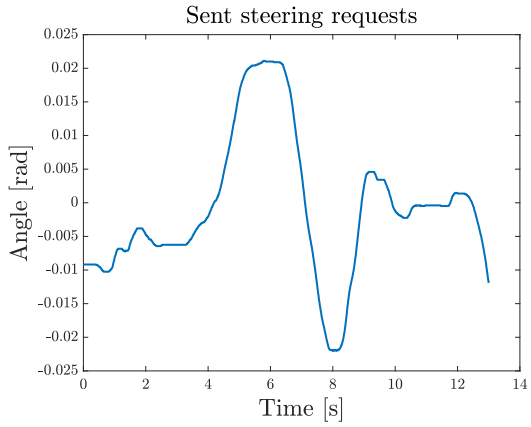

Figure 4.1: Steering angles used for the single lane change manoeuvre at 22.167 m/s.

From figure 4.2 one can notice that the linear single-track model captures the same behaviours as the real test data albeit with a higher yaw-rate. However, the VTM-model shows much higher yaw-rates. This is even clearer in figure 4.2d when the Target 2 values are in the same figure.

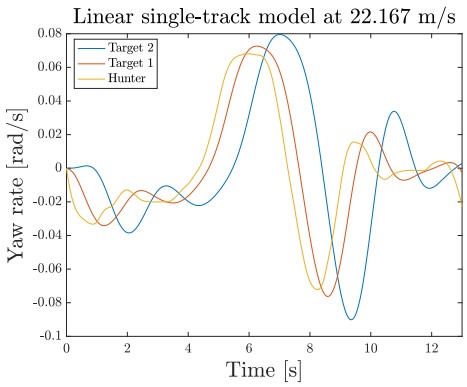

(a) Single-track model

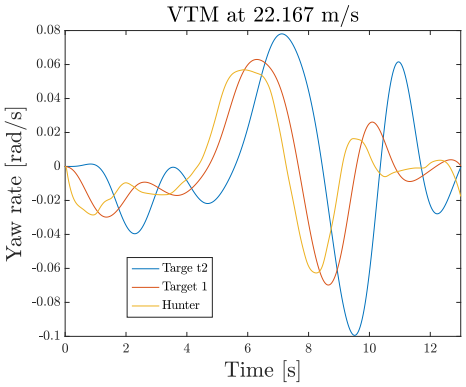

(b) VTM

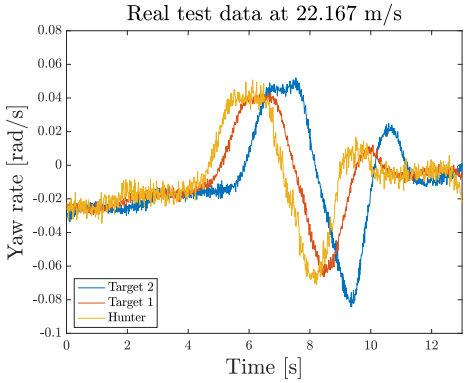

(c) Real test data

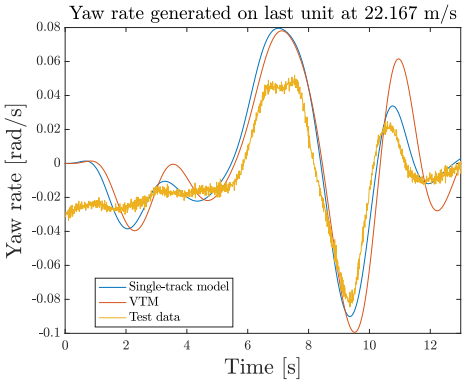

(d) Yaw-rates on last unit

Figure 4.2: Single lane change manoeuvre performed at 22.167 m/s. Figure 4.2a shows the yaw-rates generated from the linear single-track model and 4.2b from the VTM model. Figure 4.2c shows the yaw-rates from the real test data during the single lane change manoeuvre at 22.167 m/s. Figure 4.2d shows the yaw-rates generated on the last trailer from the manoeuvre.

4.3 Double lane change manoeuvre

The double lane change is similar to the single lane change manoeuvre. During double lane change manoeuvre, the vehicle steering to the adjacent lane and later steering back to the original lane. It can represent collision avoidance manoeuvre, and later steer back to the old lane. Figure 4.3 shows the steering angles used to perform the manoeuvre.

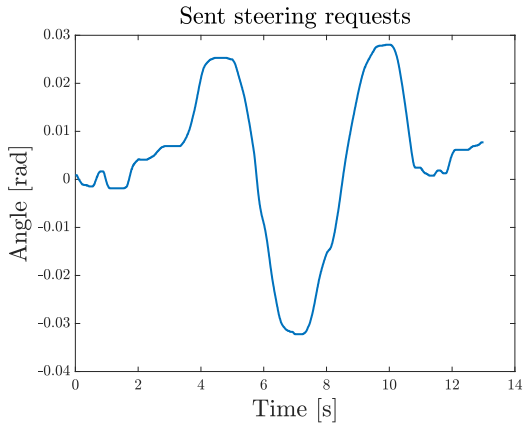

Figure 4.3: Steering angles used for the double lane change manoeuvre at 22.144 m/s.

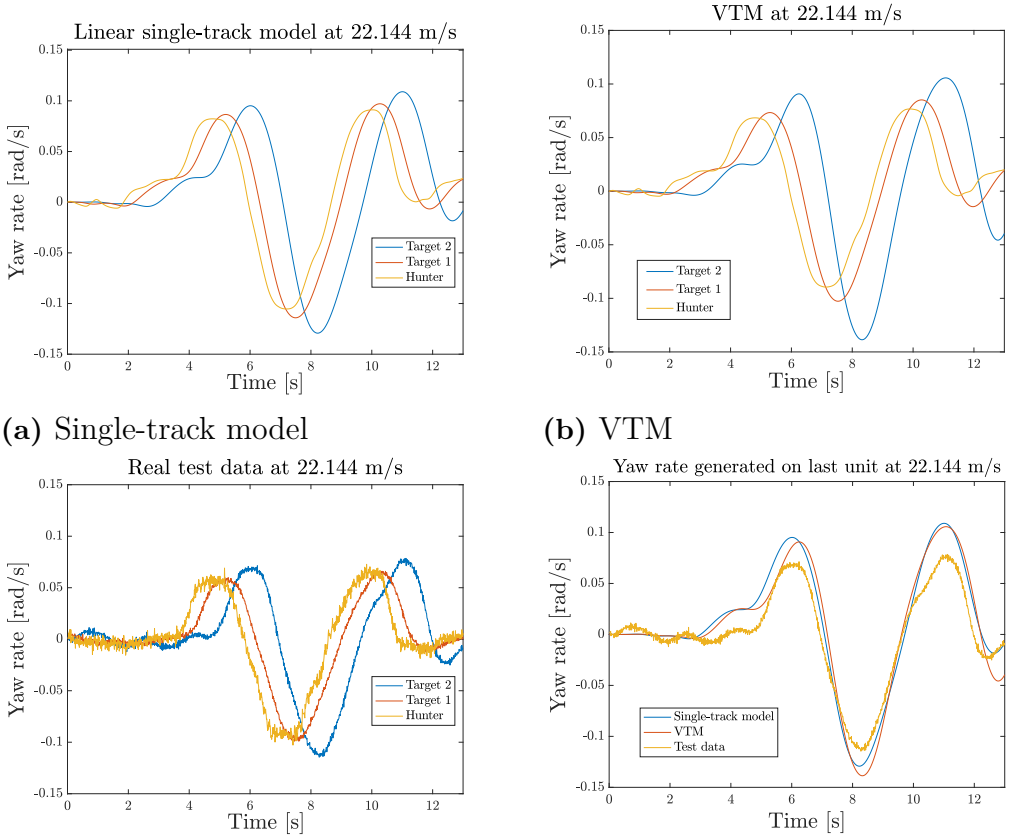

(a) Single-track model

(b) VTM

(c) Real test data

(d) Yaw-rates on last unit

Figure 4.4: Double lane change manoeuvre performed at 22.144 m/s. Figure 4.4a shows the yaw-rates generated from the linear single-track model and 4.4b from the VTM model. Figure 4.4c shows the yaw-rates from the real test data during the double lane change manoeuvre at 22.144 m/s. Figure 4.4d shows the yaw-rates generated on the last trailer from the manoeuvre.

In figure 4.4 one can notice that the linear single-track model manages to capture the

general behaviour of the test data, albeit with some deviations and higher yaw-rates. The VTM shows the same characteristics as the test data but the tractors and the first semitrailer displays slightly larger values compared to the linear single-track model and the test data. Figure 4.4d shows that the values differ less than for the single lane change manoeuvre.

4.4 Steady-state cornering

Steady-state cornering is a test where the vehicle is accelerated to a certain speed on a circular track, and measured for a certain time period whilst maintaining the vehicle at the steady state. The key point is to maintain a fixed steering angle during circling around a given radius while maintaining the same speed.

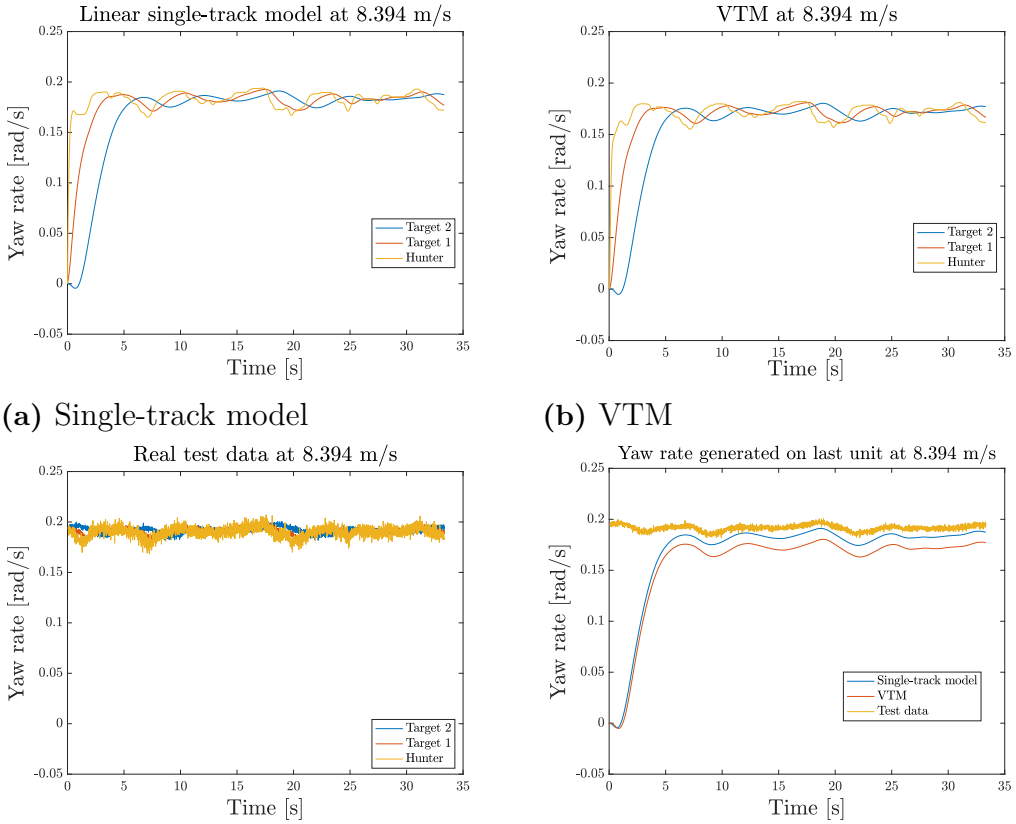

(a) Single-track model

(b) VTM

(c) Real test data

(d) Yaw-rates on last unit

Figure 4.5: Steady-state cornering performed at 8.394 m/s. Figure 4.5a shows the yaw-rates generated from the linear single-track model and 4.5b from the VTM model. Figure 4.5c shows the yaw-rates from the real test data during the steady-state cornering at 8.394 m/s. Figure 4.5d shows the yaw-rates generated on the last trailer from the manoeuvre.

One quickly notices from figure 4.5 is that the VTM and the linear single-track model shows the same yaw-rate trends. However, figure 4.5d shows that the linear single-track model converges to values close to the real test data while the VTM do not. Figure 4.5 is just one test at a certain speed at one direction.

4.5 Step-steer manoeuvre

The step-steer manoeuvre can be viewed as quickly dodging an object on the road or having to turn quickly for some reason. Figure 4.6 shows the steering angles used to perform the manoeuvre.

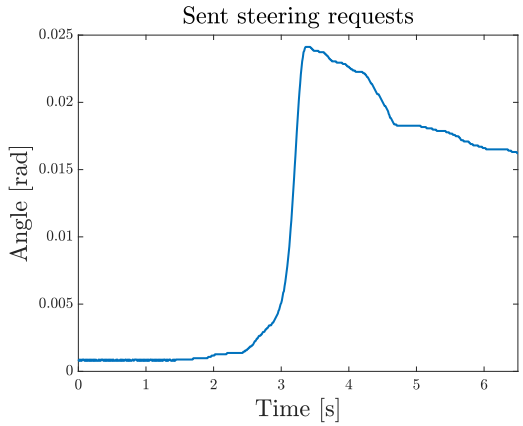

Figure 4.6: Steering angles used for the step-steer manoeuvre at 22.159 m/s.

Figure 4.7 shows that both the linear single-track model and the VTM manage to follow the yaw-rate response from the step-steer input given from the test data. However, the VTM produces higher yaw-rates compared to what the linear single-track model manages to do and the test data shows. However, the values for the tractor and the first semitrailer seem to match the other more. Figure 4.7d shows that, unlike the previous manoeuvres, the yaw-rates produces by the VTM are similar to the linear single-track model in appearance and magnitude.

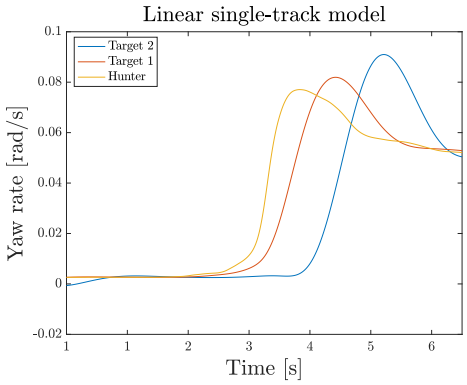

(a) Single-track model

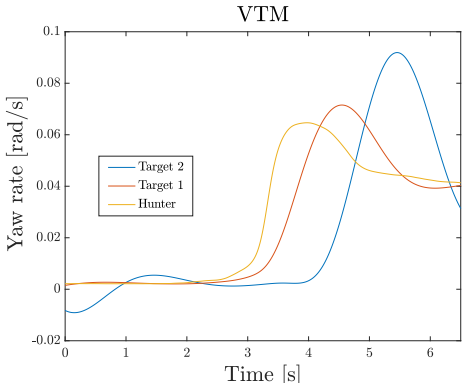

(b) VTM

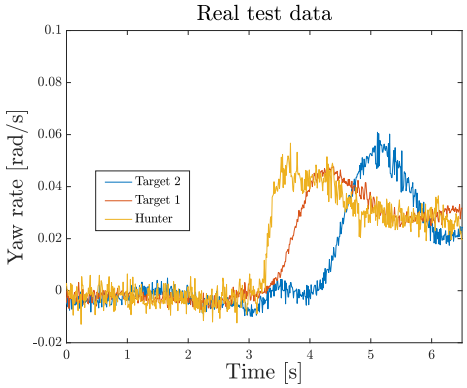

(c) Real test data

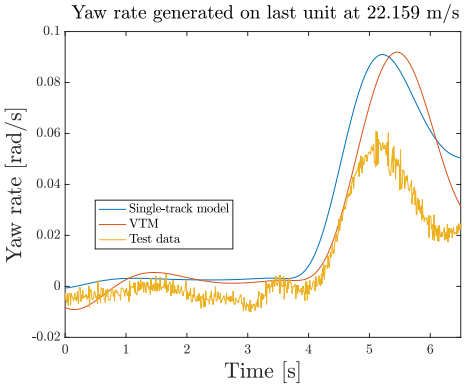

(d) Yaw-rates on last unit

Figure 4.7: Step-steer manoeuvre performed at 22.159 m/s. Figure 4.7a shows the yaw-rates generated from the linear single-track model and 4.7b from the VTM model. Figure 4.7c shows the yaw-rates from the real test data during the step-steer manoeuvre at 22.159 m/s. Figure 4.7d shows the yaw-rates generated on the last trailer from the manoeuvre.

4.6 Psuedo-random steering

According to ISO-14791 [23] a pseudo-random steering is a manoeuvre in which random steering wheel angles on the total spectrum shall not exceed four times the value of the smallest. Moreover, to acquire sufficient amount of data, the test shall proceed at least 12 minutes. The output of yaw-rates produces are then analysed using frequency analysis. One of the measures is the Magnitude Squared Coherence. Using this measure, it is possible to see at which frequencies the input signal (steering requests) stops to correlate to the output signal (yaw-rates). The other one is the Bode plot where the phase is shown in radians.

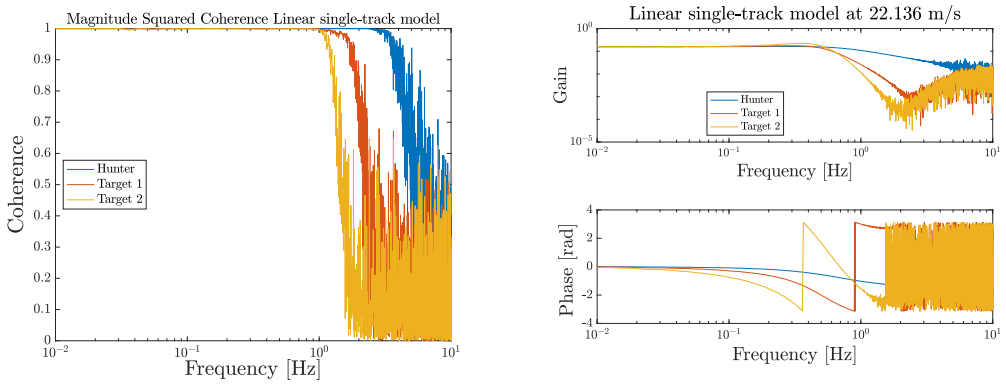

(a) Magnitude square coherence **(b)** Bode plot

Figure 4.8: Psuedo-random steering plots for linear single-track model.

Figure 4.11 showing Target 2 for the different models and test data shows that the linear single-track model looks quite similar in appearance to the VTM. That being said, the VTM loses coherence at lower frequencies as opposed to the linear single-track model, although the difference is not large. Moreover, figure 4.8a and 4.9a both fail to capture the small dip of coherence at the 0.04 Hz neighbourhood as can be inferred from figure 4.10a. The second semitrailer loses coherence faster in the real test data case than the VTM and the linear single-track model does.

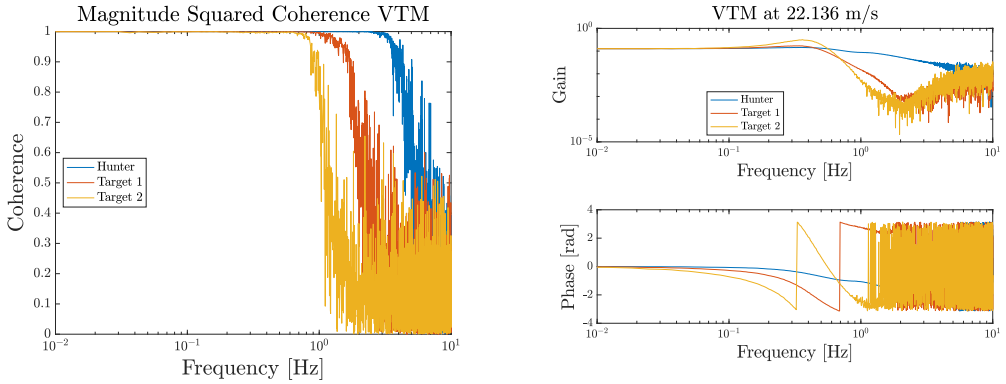

(a) Magnitude square coherence **(b)** Bode plot

Figure 4.9: Psuedo-random steering plots for VTM simulations

The Bode plots in figure 4.8b and 4.9b show that the VTM and the linear single-track model exhibits the same response to the pseudo-random steering over long periods. However, the VTM show a higher peak gain for the second semitrailer than the linear single-track model. Moreover, they do seem to show the same cut-off points. However, figure 4.11 shows that the cut-off frequencies do differ from the real test data.

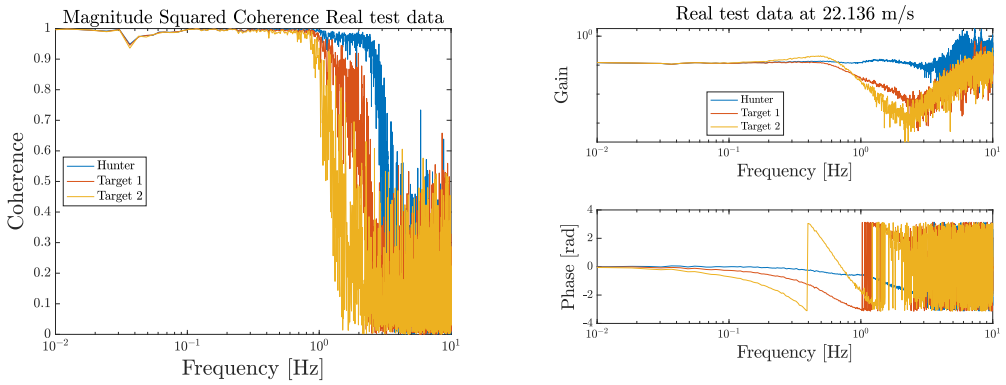

(a) Magnitude square coherence **(b)** Bode plot

Figure 4.10: Psuedo-random steering plots generated by real test data.

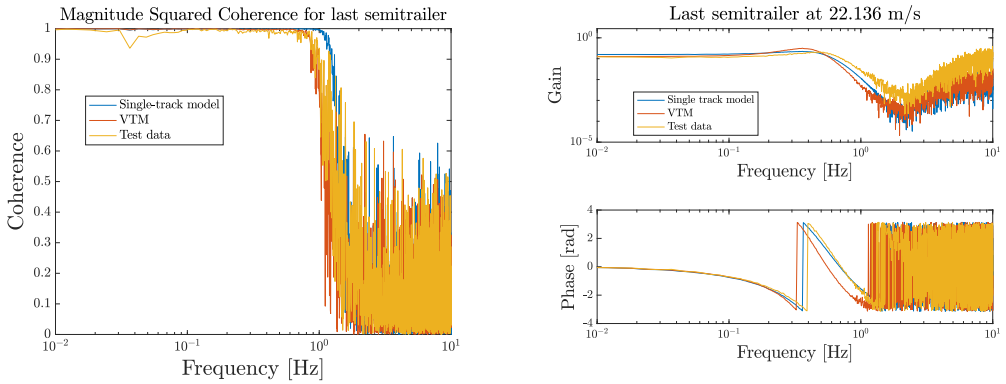

(a) Magnitude square coherence **(b)** Bode plot

Figure 4.11: Psuedo-random steering plots generated on the last trailer.

4.7 Evaluating the models

To begin with, some observations can be made by analysing the figures presented so far. The first one is that the linear single-track model and the VTM manage to capture the same behaviour as the real test data. Figure 4.2d and 4.4d shows that for the two simpler highway manoeuvres, they capture the behaviour well. However, it is worth noticing that the yaw-rates are higher than for the real data. This is clearly shown in the step-steer manoeuvre (figure 4.7d) where the linear single-track model and the VTM generate high yaw-rates, for example at the four second to seven second region. The high yaw-rates observation is also confirmed by the Bode plots in figure 4.11 where the gain is higher than the test data. The slopes observed in the beginning of figure 4.5b and figure 4.5a are likely caused by the inertia as a result of all states start with the value zero at the start of the simulation.

The second observation is that the linear single-track model loses coherence at a bit higher frequencies while the test data and the simulation results lose coherence in the same neighbourhood. The reason may be that the model do not manage to

seize road disturbances or more complex behaviours that are only found in more complex models. However, both the linear single-track model and the VTM do not show the drop in coherence that is seen in figure 4.11a. This drop along with the lower coherence of the test data might be caused by physical properties of the sensor installation on the vehicle. Furthermore, the VTMs achieved peak in magnitude occurs earlier compared with the others (figure 4.11b).

To summarize, the VTM of this particular vehicle configuration showed high yaw-rates and also exhibited the first resonant frequency earlier compared to the test data and linear single-track model. When checking the real parameter values and axle loads, it was observed that the masses for the units were incorrectly measured, and therefore the VTM was incorrectly parameterized for this study. By recalculating, a new set of axle loads and center-of-gravity positions were obtained. These corrected mass properties were used in the single-track model results presented in this section. Unfortunately the VTM could not be configured with the new estimated parameters within the given time frame due to the size and complexity of the model. The incorrect mass properties used in the VTM (which included a much lighter second semitrailer than reality) can also explain why the gain peak were located at lower frequencies than the others. Another possible explanation for the differences seen between the model-generated and the experimental data might be that the A-double used for testing is more damped than the linear single-track model and the VTM model. This could to some extent explain why the VTM and the linear single-track model showed those unwanted peaks displayed in figure 4.7d. Since the VTM model is more complex and sophisticated compared to the linear single-track model, it should outperform it in every manoeuvre if the parameters were correct. Therefore it is of interest to re-do the verification for the VTM model with the new estimated parameters as part of future work.

Realizing from the VTM that wrong parameters can have a large impact on the behaviour of the tractors, one could expect even better values the more precisely estimated the parameters are. Despite a slightly higher peak yaw-rates, the linear single-track model is able to capture most of the behaviours related to yaw of the real A-double. An interesting thing to notice is that the far more complicated VTM model does not seem to provide a significant improvement in accuracy compared to the simple linear model for these specific manoeuvres. In addition, it is of more relevance that the peaks of magnitude are located close to each other between the test data and the model, than the peaks have the same gain. The opposite case is not desirable since it would lead to incorrectly predicting when instability occurs. Considering the observations from above, a conclusion is drawn that it is possible use the linear single-track model as a valid foundation for the preventive steering controller.

5
Path follower

A path follower is a general term for an autonomous system with only one task; to follow a trajectory as well as possible. This thesis investigates different approaches to design a path follower. Their placement in the Volvo Group's functional architecture will also be presented.

5.1 Literature review

The intention of a path follower is to follow a predefined trajectory. There exists various path followers, based on different disciplines of engineering. Mitsuji Sampei et al [24] used nonlinear control theory when developing a method for arbitrary path tracking for an articulated vehicle. The use of non-linearity allows for the path follower to follow arbitrarily shaped paths. Pedro Aguiar and Joao P Hespanha [25] developed in 2007 a sophisticated path follower based on supervisory control combined with nonlinear Lyanupov-based tracking control law. Moreover, the developed method was also extended to 3-D space, thus allowing it to be used on vehicles such as hovercrafts and underwater vehicles. Hongyan Guo et al [26] developed a method which generates an envelope of maximum positions offset from the trajectory, which the tractor keeps inside while trying to follow a set trajectory with a horizontal path tracking method of choice. J-M Park et al [27] used Model Predictive Control (MPC) to create an obstacle avoiding system for autonomous vehicles.

Another approach is to use geometry as a basis for the path follower. The oldest of those algorithms is the pure pursuit algorithm. Published in 1985 by Wallace et al [28], the method uses simple geometry to calculate a requested curvature needed to reach a pre-defined goal point. Myung-Wook Park et al [29] created an adaptive version of the algorithm, allowing it to adjust the vehicles speed and look-ahead distance depending on the curvature of the road ahead.

5.2 Traffic situation management

The traffic situation management (TSM) is the functional domain that is responsible for path planning and path following in Volvo Group's functional architecture. The TSM contains the main trajectory generation and path follower functionality and generates the needed acceleration and steering request to follow the trajectory. The path follower presented in section 5.1 can be viewed as a mock TSM. It operates as a function to send longitudinal acceleration and path curvature requests to the Vehicle Motion Manager (VMM) module. In the mock TSM, the path follower algorithm utilises a kinematic model of the vehicle to estimate the needed requests. This representation of the TSM's path follower is deliberately simplified and does not accurately reflect the full TSM functionality. In addition the the current longitudinal acceleration and path curvature requests the TSM also provides preview information to the VMM. This information represents the TSMs intentions for the upcoming time points.

5.3 Volvo Group's functional architecture

The system architecture is shown in figure 5.1. The TSM sends the path curvature requests (which for small steer angles and low lateral tyre slip can directly relate to a front steer angle request) and longitudinal acceleration requests to the VMM. This is done by interpreting the traffic situation and the oncoming road curvature. A simpler mock version of the TSM will be used instead of the state-of-the-art TSM present at Volvo GTT when testing controllers. The most important feature of the TSM is the lack of access to as many of the vehicle motion states as the VMM. Thus, the TSM can be viewed as a naive driver. The Global Force Generator (GFG) reads the requests from the TSM, adjusts it with feedback from the plant, considering drag forces, such as rolling resistance, air drag and road slope, and outputs the target global forces that the vehicle's actuators should provide. The global force request is sent to the control allocator. The control allocator then passes the appropriate signals to the actuators, which could be the brake system, steering and propulsion. These actuators then act on the plant, via forces and torques. The procedure described is illustrated in figure 5.1. As it is designed at the moment, the TSM is based on a kinematic model whilst the VMM uses a dynamical model. Therefore there exist a need for a method which can check that the requests sent from the TSM are sensible and do not generate undesired instability as one could have predicted from a dynamical model.For more detail relating to the functional architecture described here readers are directed to [30].

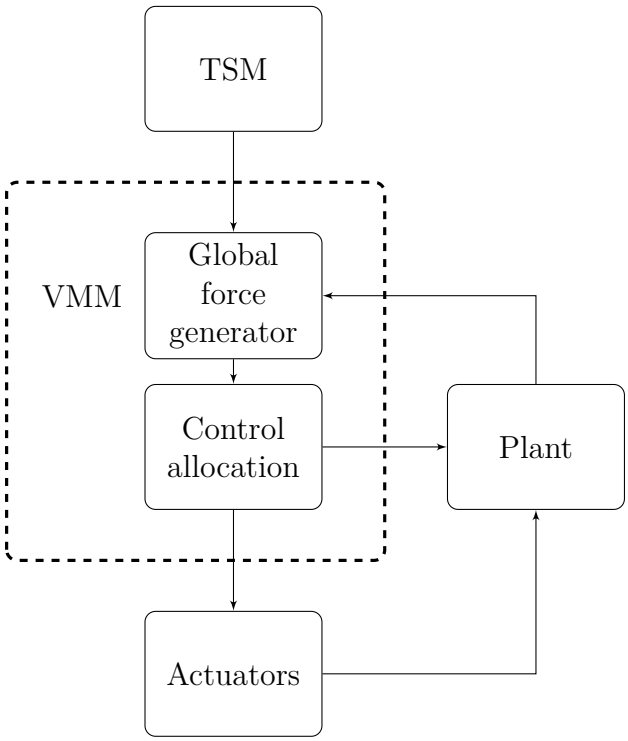

Figure 5.1: Architecture used as a base for the controller.

6

Rearward Amplification Reducing Controller

In this chapter, a proposed solution is presented alongside the idea behind it as well as how it will behave. In order to compare the performance of the controller, a benchmark has to be created. The benchmark consists of a filter, either a notch filter or a low-pass filter, which is applied to the steering request (which would come from the path follower in an autonomous vehicle).

6.1 Information search

Previous work has shown that the choice of trailers, combinations and load transfer ratios do indeed influence the lateral dynamics of LCVs [10] [31]. To reduce the RWA ratio, various active control strategies are under research, such as an automatic brake control system by braking the trailers [32], actively steered trailers [33] or by using a stochastic optimization algorithm to control the steering [34]. Sogol Kharazzi developed an eigenstructure-assignment controller to alter the modal composition of a system [35]. She also considered to adopt a MPC as a base for the control scheme. Tushita Sikder [36] used a Linear Quadratic Regulator (LQR) to increase the lateral stability of a LCV. However, most of the authors assume that there exists a steering input from a human driver. One exception is Laszlo Palkovics et al [37], who applied a LQR to create a stability controller. The stability controller used a feedback loop and steered using the rear wheels and the trailer wheels of a tractor semitrailer.

6.2 Integration of controller into the architecture

The rearward amplification reducing controller, nicknamed the “Sanity checker”, can be integrated into the system in two separate ways (figure 6.1). This thesis work will focus on the architecture shown in figure 6.1a which will be described comprehensively in section 6.3, while figure 6.1b offers an alternative concept that will be briefly described in this section.

In the non-integrated TSM approach, as shown in figure 6.1a , the sanity checker is placed in-between the TSM and the GFG. In the TSM integrated approach, the controller is integrated to the TSM and let them communicate with each other. This

is to let them eventually come up with a request they both will "shake hands" on. The request will then be sent out to GFG seen in figure 6.1b.

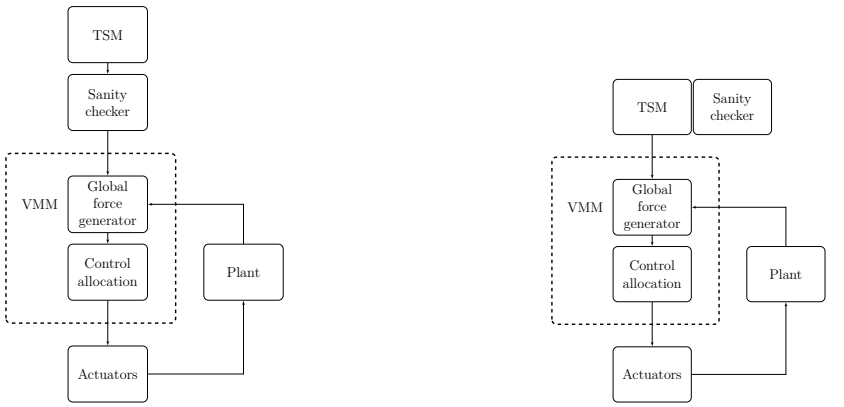

(a) Non-integrated TSM approach **(b)** TSM integrated approach

Figure 6.1: Two different types of architecture for the sanity checker.

6.3 The rearward amplification reducing controller

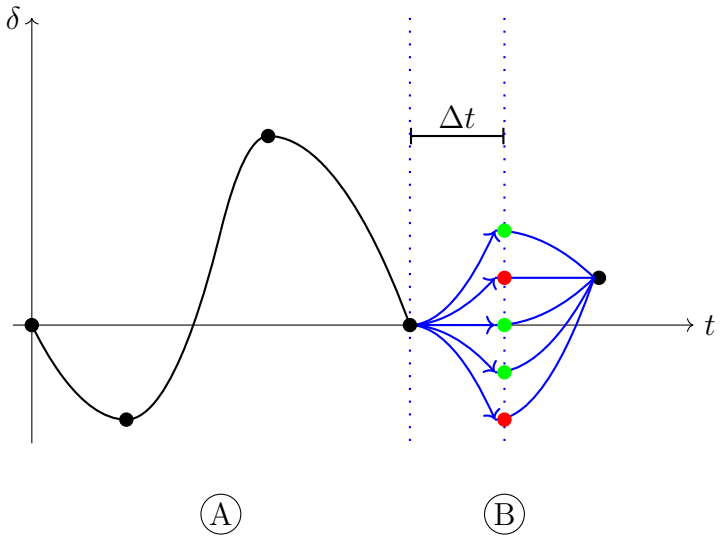

Figure 6.2: A more explicit showing of how the sanity checker works. δ is the steering requests and t is the time. Δt is the preview time distance.

The sanity checker is built by an offline part and an online part. The offline part consists of pre-computed matrices for the linear single-track model of the vehicle of interest. The model then works in the following order:

1. The model takes the preview δ_{prev} sent from the TSM, shown in part A of figure 6.2. The preview δ_{prev}

$$\delta_{\text{prev}} = [\delta_1, \delta_2, \ldots, \delta_n], \tag{6.1}$$

contains the preview points from the first oncoming point until n-steps ahead with a specified time preview step in-between them. At the start of driving, the algorithm will not begin until it has acquired n preview points from the TSM.

2. To compute the states at the end of the preview, the ordinary differential equation

$$\dot{\vec{x}} = A\vec{x} + B\vec{u}, \tag{6.2}$$

has to be solved. The matrices A and B are obtained from the equation system calculated from the A-double model in section 2.4. The ODE-solver implemented was a variable-step solver, so that even if coarse preview points are provided, the simulation of the A-double model should still capture the necessary vehicle dynamics. $\vec{u}$ is the input vector containing a steering request for a specific time point. The steering request is changed to a new value once the next time step is calculated.

3. When the states at the second to final preview point has been computed, a new set of points, **S** , are generated at placement of the n-1 preview point, shown in part B. The other preview points remain unmodified and are used when solving the ODE to acquire the states throughout the given preview. The points are evenly spread to cover a range of possible steering inputs at that time point. The range of points were chosen from a span with an upper and a lower boundary value β_+, β_- of

$$\beta_\pm = \delta_{n-1} \pm z, \tag{6.3}$$

where $z \in \mathbb{R}$ is a value chosen in advance.

4. If the distances between the preview points are too large, points in-between will be created by linear interpolation to get a more detailed curve. Two thresholds, T_{RWA} and $T_{\dot{\phi}}$, are defined for the maximum allowed RWA and the maximum allowed yaw-rate for the last unit.
5. The states at δ_n with these new points are then computed. If the yaw-rate of the last unit or the rearward amplification generated with these preview points is too high at a certain point, it will be censored (marked in red) as shown in part B. These censored points will not let steering requests matching those values pass. Instead, the steering request value will be re-directed to the closest permitted steering value if the distance (γ in algorithm 1) to a censored one is too close.
6. The algorithm proceeds by taking the next furthest preview point generated once the closest preview point is passed. The path follower appends it at the end of the array while the first element in the array is removed. This leads to the steering request at δ_{n-1} to be placed at δ_{n-2}. From there the algorithm starts over again.

This is done continuously throughout the driving session. A shorter explained version of the controller described in pseudo-code can be found in algorithm 1.

while *Pathfollower is running* **do**
  Get preview-array;
  Generate set of new points **S**;
  for *each point* **do**
    overwrite δ_{n-1} with new set point $\Omega \in$ **S**=linspace(β_-,β_+,# points) ;
    calculate the states at δ_n;
    calculate RWA;
    get $\dot{\phi}$;
    if $RWA \geq T_{RWA}$ *or* $\dot{\phi} > T_{\dot{\phi}}$ **then**
      $\Omega = -1000$;
    end
  end
  find closest value γ to δ_{n-1} from **S**;
  if $\gamma \leq 0.05$ *and* $\Omega = -1000$ **then**
    rewrite δ_{n-1} to the closest allowed in set **S**;
  end
end

Algorithm 1: Algorithm describing the sanity checker

6.4 Low-pass Butterworth filter

The low-pass Butterworth filter belongs to the class of low-pass filters. A low-pass filter allows signals below a certain frequency to pass through, while the other frequencies output signals are reduced in magnitude. By selecting a cut-off frequency that is lower than the frequencies where the RWA violation occurs, steering inputs that would potentially result in large RWA can be removed. The idea behind the Butterworth filter is to try and flatten out the magnitude peaks observed from the Bode plots. One drawback of using such a low pass filter is that it will also result in some phase lag, which may disrupt the path followers ability to closely follow a path [38]. Using Matlab's Butterworth filter function, two independent parameters are needed: the order of the filter and the cut-off frequency. The order of the filter was chosen to the highest possible order whilst still retaining sensible results. The cut-off frequency was chosen to be the eigenfrequency corresponding to the mode with large trailer yaw rates obtained from equation (3.2). The obtained eigenfrequency for the last trailer was 0.4903 Hz.

6.5 Notch filter

A notch filter, or a band-stop filter, is a simple filter which removes unwanted frequencies from a signal within a predefined frequency interval. Like the low-pass filter, the idea is that by removing frequencies that may result in high RWA, the ratio would produce a value closer to one. The drawback of using it is that it will result in some phase lag which is not desirable when running in real-time [39]. When using the Matlab notch filter function, three independent parameters are needed: the order of the filter, the lower band-stop filter frequency and the higher band-stop frequency. The upper and lower band-stop frequencies were chosen such that they try to remove all the unwanted frequencies. Another way to do this is to calculate the eigenfrequency for the last trailer using equation (3.2) and choosing a neighbourhood around it. The obtained eigenfrequency for the last trailer was 0.4903 Hz. By trial and error, the order of the filter was chosen to be the highest order possible without letting the results diverge to infinity.

7
Results

In this chapter the results are presented. It covers the resulting yaw-rates generated from a set of steering requests, used in section 4. In addition, results from the notch filter and Butterworth filter are also presented for comparison.

7.1 Generation of results

To get comparable results between the different methods, a rigid testing procedure has to be created. As discussed in section 4.7, the VTM-model could not be used for validation of the controller in this work. The procedure used to generate results for different RWA reduction methods is shown in figure 7.1. The steering requests are created from the real life manoeuvres recorded in Section 4. These requests are then converted to steering angles. The steering requests are sent to one of the filters or the sanity checker where the requests are modified. From there, the requests are fed through the linear single track model to acquire the yaw-rates. These yaw-rates, combined with the RWA, will be the qualitative measurement used to assess the performance of the methods.

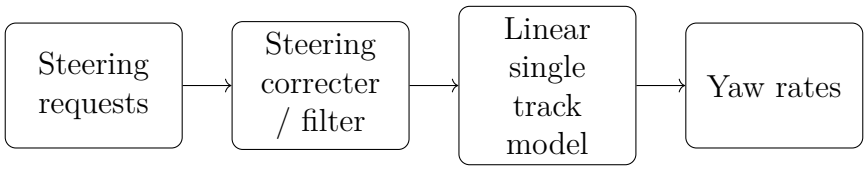

Figure 7.1: Illustration of how results are generated.

The unfiltered case is the result obtained from removing the second block in figure 7.1, i.e, not altering the steering requests. The following results assume a constant speed of 22 m/s. The controlled case is the result obtained using the sanity checker described in section 6.3. The steering requests coming from a human driver, sampled at 10 ms, will have to be converted to TSM-equivalent preview points steering angle requests. This is done by first downsampling the requests to a new sample rate (the preview time distance), before being treated by the sanity checker. After being processed, the new steering requests were upsampled again through linear interpolation to the original sample rate. RWA threshold T_{RWA} used here is 1.1 and yaw-rate threshold $T_{\dot{\phi}}$ is 0.1363 [rad/s]. The default preview points were chosen to be seven. For the Butterworth filter and the notch filter, the parameters were chosen according to section 6.4 and 6.5. The values are shown in table 7.1.

	Order	Cut-off frequency [Hz]	Lower bandstop frequency [Hz]	Upper bandstop frequency [Hz]
Butterworth filter	3	0.4903	-	-
Notch filter	2	-	0.35	0.75

Table 7.1: Parameters used for each filter when producing results.

7.2 Single lane change

The single lane change manoeuvre applied to produce the results is the same one used for verifying the linear single-track model in 4.2. Figure 7.2 shows the steering requests used to produce the yaw-rates in figure 7.3. The steering requests were generated in the way described in section 7.1.

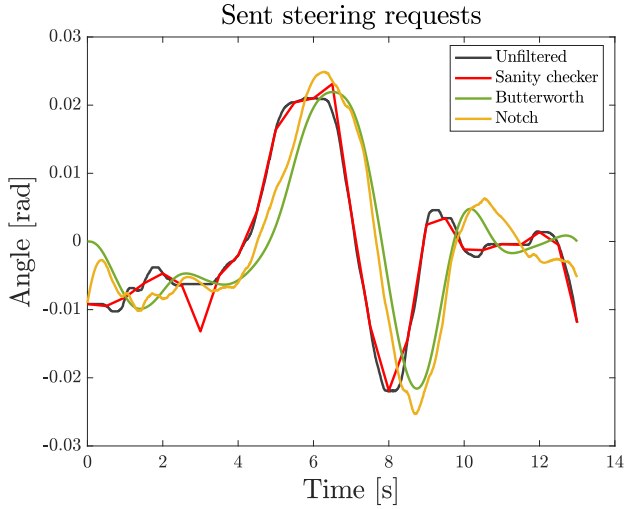

Figure 7.2: Steering requests sent from different method for the single lane change manoeuvre.

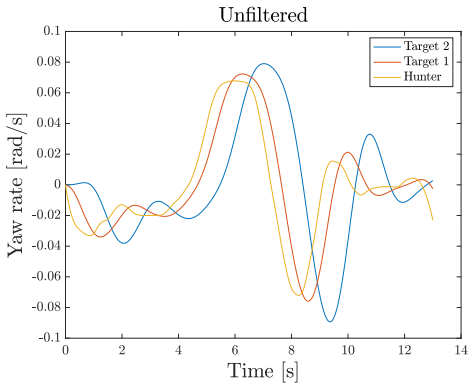

(a) The unfiltered case

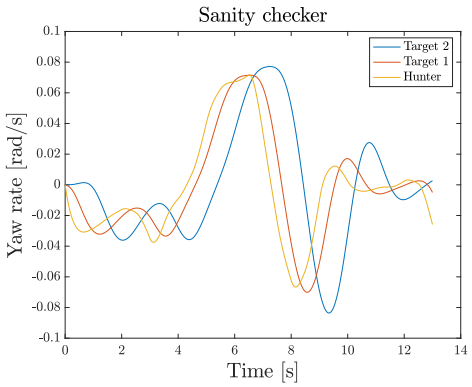

(b) Sanity checker

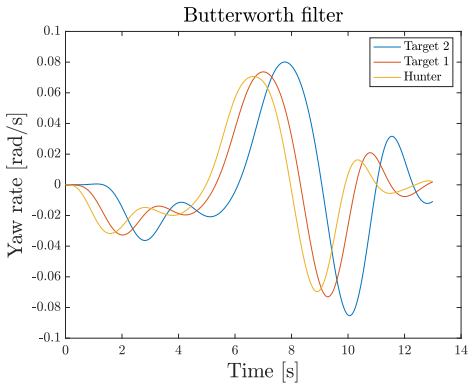

(c) Butterworth filter

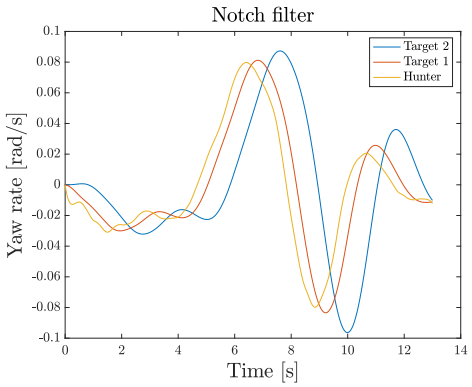

(d) Notch filter

Figure 7.3: Yaw-rates generated from different methods for the single lane change manoeuvre.

7.3 Double lane change

The double lane change manoeuvre implemented to produce the results is the same steering request as in figure 4.3. Figure 7.4 shows the steering requests used to produce the yaw-rates in figure 7.5. The steering requests were generated in the way described in section 7.1.

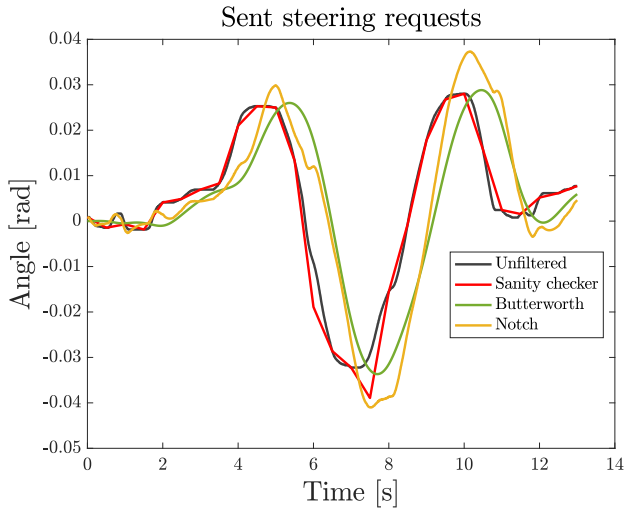

Figure 7.4: Steering requests sent from different method for the double lane change manoeuvre

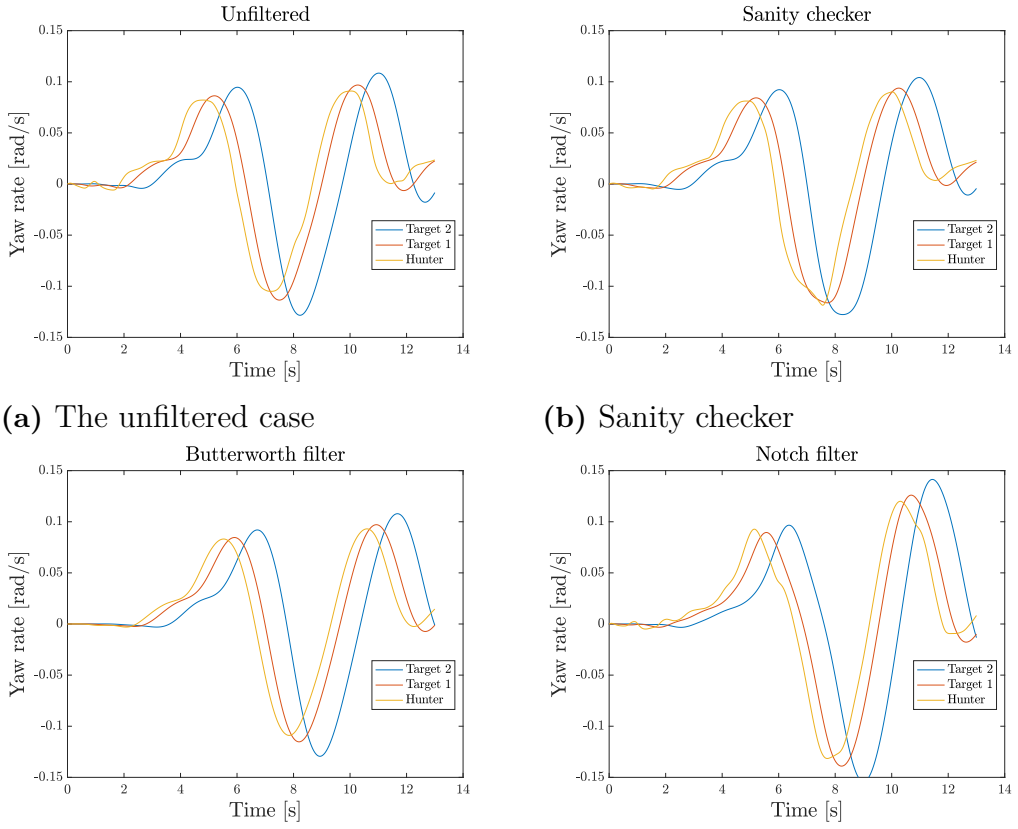

(a) The unfiltered case

(b) Sanity checker

(c) Butterworth filter

(d) Notch filter

Figure 7.5: Yaw-rates generated from different methods for the double lane change manoeuvre.

7.4 Step-steer

The steering angles to generate the yaw-rates for the step-steer manoeuvre are shown in figure 4.6. Figure 7.6 shows the steering requests used to produce the yaw-rates in figure 7.7. The steering requests were generated in the way described in section 7.1.

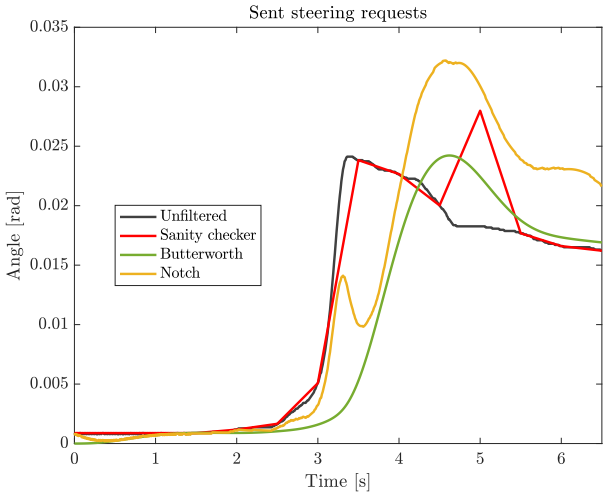

Figure 7.6: Steering requests sent from different method for the step-steer manoeuvre.

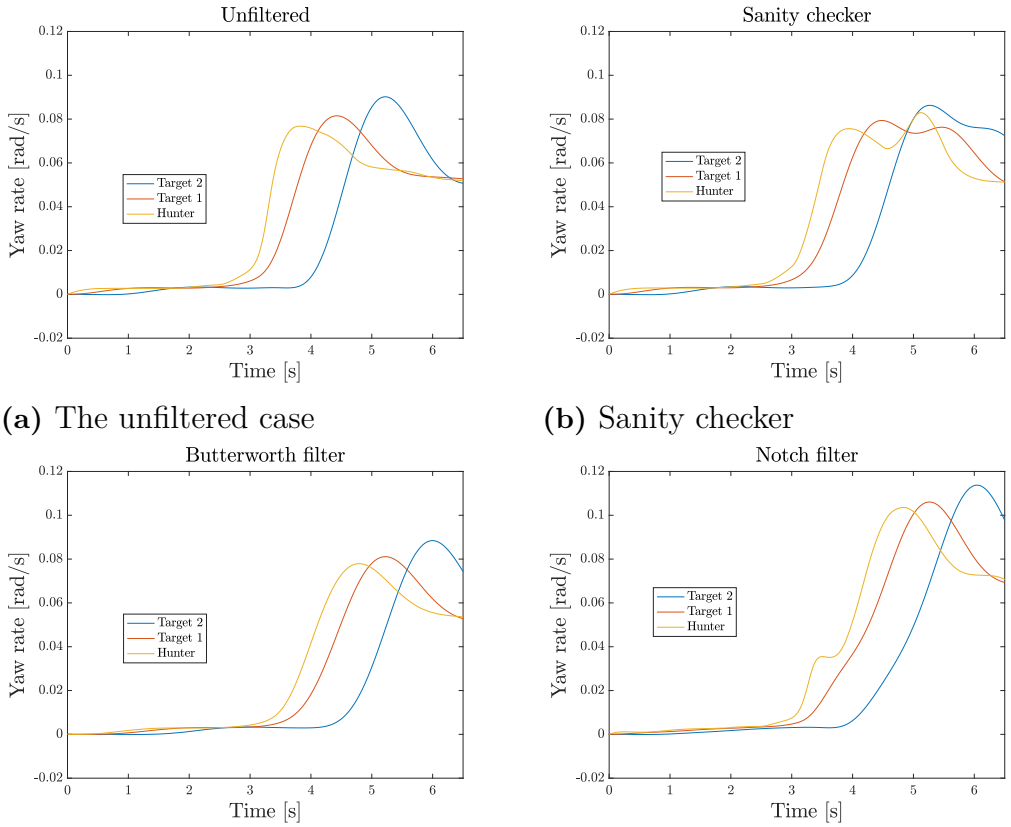

(a) The unfiltered case

(b) Sanity checker

(c) Butterworth filter

(d) Notch filter

Figure 7.7: Yaw-rates generated from different methods for the step steer manoeuvre.

7.5 Resulting rearward amplification

The yaw-rates generated during the simulation method were logged. Using equation (3.1) the RWA ratio was calculated. Table 7.2 presents the rearward amplification ratio generated for each method including the unfiltered case for all manoeuvres for a preview time distance of 500 ms and seven preview points.

	SLC		DLC		SS	
	RWA	Yaw-rate	RWA	Yaw-rate	RWA	Yaw-rate
Unfiltered steering	1.1726	0.0893	1.1708	0.1284	1.1749	0.0902
Sanity checker	1.1655	0.0836	1.0774	0.1277	1.0405	0.0863
Butterworth filter	1.2080	0.0853	1.1875	0.1294	1.1349	0.0884
Notch filter	1.2074	0.0964	1.1726	0.1542	1.0983	0.1137

Table 7.2: Rearward amplification and absolute maximum yaw-rate [rad/s] observed on the last unit generated from different manoeuvres. SLC stands for single lane change, DLC stands for double lane change and SS stands for step-steer.

7.6 Resulting rearward amplification for different number of preview points

Table 7.3 shows the generated RWA from the single lane change manoeuvre for different amounts of preview points. The chosen preview time distance was 500 milliseconds between preview points.

Number of preview points	2	3	4	5	6	7	8	9	10	11
RWA	1.1241	1.1971	1.2534	1.1691	1.1673	1.1655	1.1669	1.0690	1.1644	1.1644

Table 7.3: Rearward amplification generated from different amount of preview points.

7.7 Resulting rearward amplification for different sizes of preview time

Table 7.4 shows the generated RWA generated from the single lane change manoeuvre for different preview time distance between the preview points. The amount of preview points was seven.

Preview time [ms]	100	200	300	400	500	600	700	800	900	1000
Sanity checker	1.2529	1.3217	1.2192	1.2610	1.1655	1.1347	1.1278	1.0965	1.0924	1.0848

Table 7.4: Rearward amplification generated from different preview time distances.

7.8 Resulting rearward amplification for different sizes of preview time and number of preview points

Table 7.4 shows a more comprehensively generated RWA constructed from the single lane change manoeuvre. It includes a grid for different amounts of preview points for a certain preview time distance between the points.

PT [ms] /PP	2	3	4	5	6	7	8	9	10	11
100	1.1906	1.2980	1.2738	1.2760	1.2740	1.2529	1.2528	1.2533	1.2882	1.2746
200	1.1774	1.3410	1.3153	1.3330	1.2643	1.3217	1.3180	1.3217	1.3115	1.2570
300	1.1799	1.2679	1.2367	1.2651	1.2633	1.2192	1.2340	1.2248	1.2372	1.2393
400	1.1256	1.2560	1.3103	1.2029	1.2565	1.2610	1.2637	1.2633	1.1523	1.2466
500	1.1241	1.1971	1.2534	1.1691	1.1673	1.1655	1.1669	1.0690	1.1644	1.1644
600	1.2411	1.2378	1.1866	1.1869	1.2345	1.1347	1.1347	1.1347	1.1347	1.1347
700	1.1752	1.1816	1.1262	1.1264	1.1308	1.1278	1.1246	1.1246	1.1246	1.2310
800	1.1150	1.1014	1.1025	1.0965	1.0965	1.0965	1.0965	1.0965	1.1463	1.1463
900	1.0928	1.0841	1.0924	1.0924	1.0924	1.0924	1.0924	1.1151	1.1151	1.1524
1000	1.1040	1.0879	1.0724	1.0848	1.0848	1.0848	1.1096	1.1117	1.1014	1.1014

Table 7.5: Rearward amplification generated from different amounts of preview points and size of preview time distance. PP is the abbreviation of preview points and PT the preview time.

7.9 Extreme case

An extreme case is also presented. The case consists of several single lane changes with large steering angles following each other. The only method tested in this case is the sanity checker. In this case the sanity checker used a preview time distance of 500 ms with seven preview points. The steering requests are found in figure 7.8. The resulting yaw-rates are showing in figure 7.9. Table 7.6 shows the RWA and largest observed yaw-rate from the manoeuvre. Tables showing the generated RWA values for different amount of preview points and preview time distance are found in Appendix A.2. Likewise, a similar table instead showing the largest observed absolute yaw-rate are found in the same section.

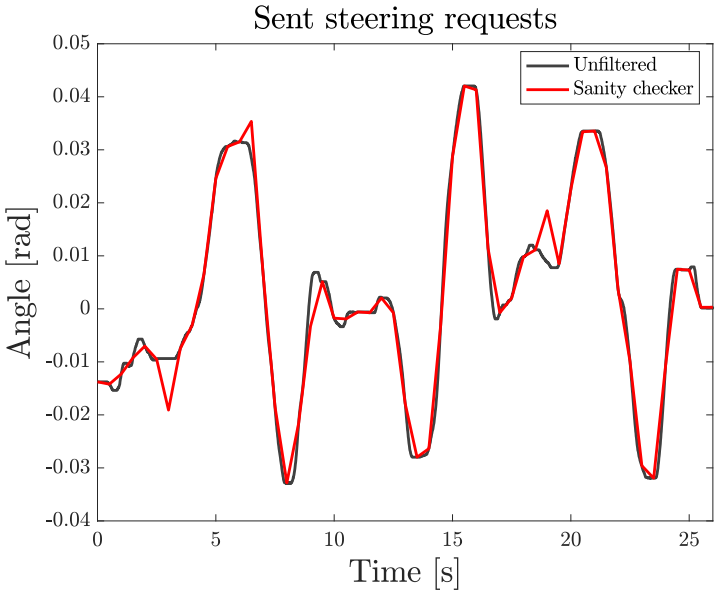

Figure 7.8: Steering requests sent from different method for the extreme case.

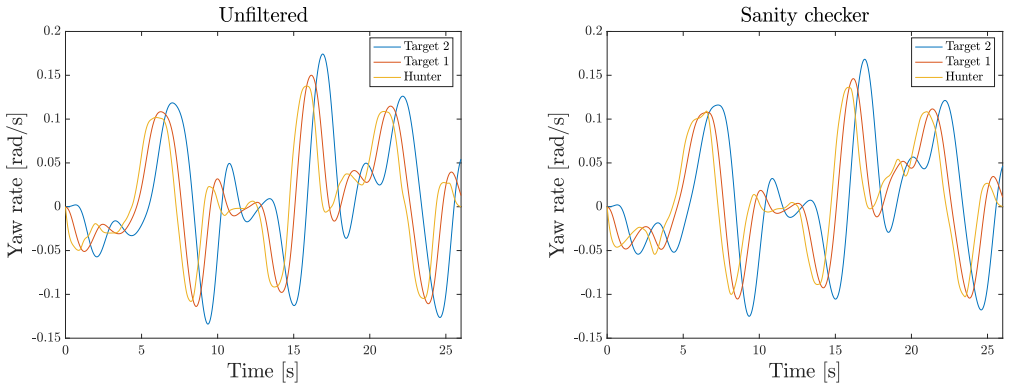

(a) The unfiltered case **(b)** Sanity checker

Figure 7.9: Yaw-rates generated from different method for the extreme case.

Case/Manoeuvre	RWA	Yaw-rate
Unfiltered steering	1.2657	0.1742
Sanity checker	1.2346	0.1683

Table 7.6: Rearward amplification and absolute maximum yaw-rate[rad/s] observed on the last unit generated from different manoeuvres.

8
Discussion

In the following chapter a more in-depth discussion about the sanity checker is presented. The performance of the controller, the benefits and the drawbacks are among the topics adressed. The chapter will attempt to answer the questions asked in the project description in section 1.2.

8.1 Performance of Sanity checker

From table 7.2 it becomes clear that the sanity checker reduces RWA compared to the unfiltered case. Moreover, it also outperforms the low pass Butterworth filter and the notch filter. This is especially clear when looking at the double lane change and step-steer manoeuvre.

An interesting observed characteristic of the sanity checker when looking behind the RWA numbers in all the three manoeuvres, is the way the method choses to reduce the RWA. From equation 3.1 we know how the ratio is defined. The most sensible and intuitive way of moving a ratio towards one when talking about vehicle dynamics is to reduce the highest value towards the lowest. However, the sanity checker instead chooses to increase the yaw-rate of the tractor in an effort of trying to get the RWA close to one, as in the case of figure 7.5b. Table 7.2 tells us that the tactic certainly works. This tactic is valid since it keeps itself within the defined yaw-rate threshhold set to 0.1363 rad/s for the last unit and is a proof that the sanity checker works. However, from a traffic safety standpoint this undesirable as it would not reduce the risk on the last semitrailer, but increase the risk of the first tractor. Figure 7.2, 7.4 and 7.6 all show that the filters suffer from a lag after filtering. This is one drawback of utilizing filters. That is, one loses the direct response from the steering. Whilst the Butterworth filter somewhat leads to the same yaw-rate characteristics as the unfiltered one, the notch filter gives distorted yaw-rates. One may notice that the yaw-rates generated by the notch filter are far higher than the other yaw-rates from the Butterworth filter. This is happening even though the RWA shows that it should be ”safer” than the Butterworth filter, which is the issue with solely focusing on RWA. It is again worth mentioning that the thesis does not focus on filter-tuning. Therefore, the filters could potentially be tuned to better performance.

An interesting observation is the fact that increasing the number of preview points is not a guarantee to achieve better performance. Looking at table 7.5 one can detect that the sample rate often has a larger impact than the number of preview points, as

also shown in table 7.4. Using more preview points help to some extent, but without a larger preview-time distance in-between, the sanity checker loses sight of what is happening further down the road, which leads to a poorer planning. A further inspection reveals that a combination of larger preview time distance combined with a lot of preview points tend to produce low RWA values. This it is not surprising since it corresponds to knowing more about the oncoming trajectory, therefore giving the sanity-checker more time to plan the total manoeuvre.

Knowing that the significance of the number of preview points is not as important as the preview time distance is valuable knowledge when implementing the controller for real testing. To save computational time, one could cut down on the number of preview points. However, it is a fine balance since having too large preview-time distance will lead to the loss of detail in the steering requests. Furthermore, larger distance between the points result in more time spent interpolating when returning to the original sample rate. A mixture of those is therefore desirable since just looking at the RWA is not looking at the whole picture. A lower RWA, as discussed previously, does not tell the whole truth. The loss of detail by using larger preview-time distance might therefore lead to a more unsafe behaviour in practice.

A method fair to compare the sanity checker with, would be the MPC. At first glance, MPC seem similar to the sanity checker. It is designed for real-time applications which makes use of a preview horizon together with a state-space model of the vehicle. Having said that, there are some fundamental differences between the methods. The first one is that unlike MPC, the sanity checker is not an optimization method. It does not have a cost function it is trying to minimize, nor is it changing every steer request. Instead, the sanity checker should be viewed as a sophisticated filter. The sanity checker provides a grid with steering angles that are not allowed. The request will be overwritten to a sufficiently close allowed value if it should be too close to a censored value. MPC tries to optimize the steering requests at each time step for the given horizon to be as close to a reference path as possible, which is a distinct difference to the sanity checker. Performing on-line optimization is generally computationally expensive. The MPC is very hardware dependent since it performs optimization for every time-step to find the most optimal solution. The sanity checker relies on forward computing the ODE-system, which in general is much faster and simpler to compute.

This is one of the advantages of the sanity checker. It is fast, and easily integrated into the current architecture and produces improved requests without too many alterations compared to the original one. Nevertheless, there are some drawbacks. One is the amount of independent parameters. Besides the amount of preview points and preview time distance, the number of set points and the thresholds have to be decided. Also, the method is lacking a “feel” for where the A-double will end up when changing the steering requests. In a sense, the controller does not have any knowledge of its surroundings and is neither interested to know. For example, a new request could lead to the tractor turning far too aggressive which would lead to the A-double hitting nearby traffic or a guard-rail. This could happen despite the

steering request is sensible, as it is lacking an understanding of its surroundings.

Since the steering requests for the general highway manoeuvres were taken from tests done by a test driver, the requests did not risk the vehicle rolling over. Therefore, section 7.9 presents a synthetic case with more extreme request to create dangerous more dangerous driving. This is done to test how well the sanity checker performs in more extreme scenarios. The roll-over limit is usually between 3-4 m/s^2 lateral acceleration which in 22 m/s is approximately equivalent to a yaw-rate of 0.1363-0.1818 rad/s. From table 7.6 one notice that the RWA and yaw-rate are lowered. On the other hand, the lowered yaw-rate is still in the zone causing a roll-over. Looking at table 7.9 it is shown that using other amounts of preview points and preview time distances do not lower the largest yaw-rate below 0.1363 rad/s, even though the threshold set to that value. One reason this might happen is because of the sanity checkers design. It does not remember any previous steering requests, the only it remember is the present state and what will happen seven points ahead. Hence, the thresholds are only working within the preview-interval and are not used over the whole manoeuvre. For the yaw-rates to be kept below the limit, a function for the sanity-checker has to be developed which considers more of the manoeuvre, both previous event and future.

8.2 Is it possible to use a linear single-track model as a foundation for a controller designed to handle highway scenarios?

As discussed in section 4.7 a linear-single-track model could be used as a foundation for a controller. However, it requires the model to be sufficiently accurate. This includes a good estimation of the parameters (axle loads, lengths, center-of-gravity positions et cetera) and that the assumptions made on the model (constant speed, small angles) are not violated. This means that the small-angle assumption and constant speed still holds. Thus, the controller is most suitable for highway driving. Driving in lower speeds often demands greater steering angles which in turn violates small-angle assumptions. Driving at low speeds also makes the linear single-track model inaccurate and country-road/city driving often leads to changing speeds. This is one of the drawbacks of using a linear single-track model. If an A-double is driving on the highway and a new speed limit is introduced, the model has to be recalculated. Even if the matrix calculations are fast there will be a time when the sanity checker will be turned off. This could be solved by planning ahead and pre-computing the matrices, such that when the new speed is introduced the matrices are quickly replaced. One of the benefits of using a linear single-track model is that feed-forward computations are very fast to compute and with an accurate model, gives good predictions. If a non-linear model instead would be used, computational time would be increased but a better accuracy would be gained. Even though better accuracy is always welcomed, the longer computational time could render it challenging for real-time use.

8.3 Does the proposed control method reduce RWA to an acceptable level?

From table 7.2 one can conclude that the RWA is at least lowered for each single case. However, the word acceptable is not so concrete. Table 8.1 reveals that the difference is barely reduced for the single lane change whilst making significant difference for the double lane change and the step-steer manoeuvre. Looking at the difference in percentage terms, this is also confirmed. However, it is worth noting that the sanity checker ran with seven preview points and at 500 ms sample rate. Hence, there is potential for the sanity-checker to be improved. Looking at table 7.5 one can guarantee there exists lower RWA that could be reached. The same probably goes for the double lane change manoeuvre and step-steer manoeuvre.

Case/Manoeuvre	SLC	DLC	SS
Unfiltered steering	1.1726	1.1708	1.1749
Sanity checker	1.1655	1.0774	1.0455
Difference (+/-)	-0.0071	-0.0934	-0.1294
Improvement (%)	0.6 %	8.0 %	11.0 %

Table 8.1: Rearward amplification generated from different cases. SLC stands for single lane change, DLC is for double lane change and SS is for step steer. A negative difference indicates that the values are reduced by the specified amount and the same goes for improvement.

Given the right choice of parameters the method could reduce the RWA to acceptable levels. Once a defined level is chosen, one could use a table like table 7.5 to choose a set of parameters that gives a value below it. However, the other manoeuvres also have to be considered since it is not guaranteed that the corresponding parameter choice leads to RWA values that are acceptable for the others.

8.4 Does the proposed method work for all predefined highway driving scenarios?

For the method to work for highway driving, the most important aspect to consider is that the corrected steering inputs lead, in general, to similar inputs as the unfiltered one. The resulting yaw-rates on the last unit should not be much larger than the yaw-rates generated from the unfiltered case. As concluded before, the sanity checker generates lower RWA. Unlike the notch-filter where RWA is somewhat misleading, the yaw-rates stay within the same bounds as the unfiltered case seen in table 7.2. This is true for all the three manoeuvres.

Given the results at hand, the method could be suitable for highway driving scenarios. As mentioned previously, one of the requirements is that the driving is done at high constant speeds. Hence, applying the controller while the tractor is in cruise

control is one of the optimal uses.

It would be interesting to see how the new steering requests and the yaw-rates would affect the tractors positioning in Cartesian coordinates. This could unfortunately not be covered due to the far too high yaw-rates displayed on the last unit of the VTM model. The possible reasons behind it was thoroughly discussed in section 4.

8.5 Can the results of an A-double linear single-track model represent simulation or real-world testing?

As discussed in section 4 the linear single-track model manages to capture most of the behaviours of a real A-double. However, it is lacking the damping displayed in the A-double and that needs to be addressed for the yaw-rates to be further reduced. The bode plots in figure 4.11b showed that the magnitude peaks almost occur at the same frequencies. Noticing from the plots in chapter 4, the linear single-track model manages to capture the trends and the behaviour of the real test data, but usually over-estimate the magnitude of the peaks. Thus, as long as the the linear single-track model is not used to find the exact values of the yaw-rates, it can be used to capture general trends and behaviours. For example, if the model predicts predicts a large peak in yaw-rate there is a high probability this is true. This does not need to be something bad. If the model is used to prevent large yaw-rates, the controller will possess a conservative characteristic, which is better than under-estimating the peaks. The RWA ratio is still possible to estimate with good accuracy since it is a ratio between the largest observed yaw-rates. Therefore, as long as the trends/behaviours are captured and the proportions between the peaks are somewhat preserved, a linear single-track model can be used to represent simulation/real-world testing.

This is also confirmed by Bengt Jacobson et al [40], where they showed that a linear single-track model retains best accuracy for rearward amplification ratio of yaw-rates. An accuracy of $\pm 5\%$ could be achieved if it was done through linear frequency domain analysis and a $\pm 5\%$ by frequency response analysis. However, they also mention that a relaxation length should be included to the tyre model due to the impact it had on the results. Hence, a well-parameterized single-track model with improved tyre model could be used to represent simulation or real-world testing to some extent. Doing so may however make the model non-linear, therefore resulting in more complex vehicle model.

8.6 Future work

The rearward amplification reducing controller uses the RWA ratio as one of the quantitative measurement during computation. A further improvement is to include a function which encourages the controller to choose driving request leading to safer driving behaviour. At the moment, the controller only chooses steering angles on the basis of which gives the lowest RWA value. Another improvement to the controller would be to add a threshold for maximum yaw-rate observed at a certain defined interval. This would immediately eliminate the risk of having too large yaw-rates. Furthermore, it would be beneficial to include the magnitude of the yaw-rate predictions into the sanity checker. Also, adding some sort of damping to the linear single-track model could further improve the accuracy of the model.

As mentioned previously, testing to see how much the controller would make the tractor deviate from the planned trajectory is necessary. An extension of this would be to test the controller in-the-loop to see if the autonomous driving system would compensate for the deviation or not, and see if it in the long-term leads to instability. Moreover, an in-depth investigation of the effects uncertain vehicle parameters is needed to see how the characteristics change and thereafter forming a tolerance band. In terms of filter, a better tuning of the filters is necessary to get a more qualitative measure against the controller.

9
Conclusion

The rearward amplification reducing controller provides a simple yet novel working controller with potential that can be used for autonomous driving LCVs on highways. It is shown that a linear single-track model could be used as a foundation for a controller with preliminary positive results. This was validated against a VTM model and real test data of an A-double.

The controller provides an intuitive and simple design that is easily tuned. It has the advantage of not requiring access to individual control actuators on all vehicle units or using sophisticated control methods. It only needs to know the vehicle combination it is driving combined with the parameters. It was shown that it could improve the generated rearward amplification ratio whilst not distorting the steering values and yaw-rates significantly. A low-pass filter and a Notch-filter was used as comparison and was tuned using the eigenfrequencies of the linear single-track model. For the highway manoeuvres the sanity checker outperformed the filters in the majority of the cases. The notch filter was shown to distort the results too much. A finer tuning of the filters is necessary to get a more qualitative measure against the controller.

The rearward amplification reducing controller could benefit from implementing a function which encourages the controller to consider safe driving behaviour when choosing between steering requests. Testing in simulation with an autonomous driving system, is needed before any closed loop tests are done on a real vehicle.

Bibliography

[1] Umberto Montanaro et al. "Towards connected autonomous driving: review of use-cases". In: *Vehicle System Dynamics* 57.6 (2019), pp. 779–814.

[2] Toheed Ghandriz et al. "Impact of automated driving systems on road freight transport and electrified propulsion of heavy vehicles". In: *Transportation Research Part C: Emerging Technologies* 115 (2020), p. 102610.

[3] Rob Palin et al. "ISO 26262 safety cases: Compliance and assurance". In: (2011).

[4] Matthijs Klomp et al. "Trends in vehicle motion control for automated driving on public roads". In: *Vehicle System Dynamics* 57.7 (2019), pp. 1028–1061.

[5] Maliheh Sadeghi Kati. "Definitions of performance based characteristics for long heavy vehicle combinations". In: *Chalmers University of Technology, Tech. Rep* (2013).

[6] John Aurell, Thomas Wadman, and Volvo Trucks. "Vehicle combinations based on the modular concept". In: *NVF-reports, Report* 1 (2007).

[7] Md Manjurul Islam et al. *Parallel design optimization of multi-trailer articulated heavy vehicles with active safety systems*. University of Ontario Institute of Technology Ontario, Ottawa, Canada, 2013.

[8] PS Fancher and CB Winkler. "A methodology for measuring rearward amplification". In: *Proceedings: International Technical Conference on the Enhanced Safety of Vehicles*. Vol. 1992. National Highway Traffic Safety Administration. 1992, pp. 352–358.

[9] Bengt Jacobson et al. *Vehicle Dymnaics Compentium*. 2018.

[10] MFJ Luijten. "Lateral dynamic behaviour of articulated commercial vehicles". In: *Eindhoven University of Technology* (2010).

[11] Chieh Chen and Masayoshi Tomizuka. "Dynamic modeling of tractor-semitrailer vehicles in automated highway systems". In: (1995).

[12] Michael Levén et al. *Derivation of linear single-track truck-dolly-semitrailer model with steerable axles*. Tech. rep. Chalmers University of Technology, 2011.

[13] Peter Nilsson and Kristoffer Tagesson. *Single-track models of an A-double heavy vehicle combination*. Tech. rep. Chalmers University of Technology, 2014.

[14] Hans B Pacejka and Egbert Bakker. "The magic formula tyre model". In: *Vehicle system dynamics* 21.S1 (1992), pp. 1–18.

[15] Wolfgang Hirschberg, Georg Rill, and Heinz Weinfurter. “Tire model tmeasy”. In: *Vehicle System Dynamics* 45.S1 (2007), pp. 101–119.

[16] R.T Uil. “Tyre models for steady-state vehicle handling analysis”. Eindhoven University of Technology, 2007.

[17] C Canudas De Wit et al. “A new model for control of systems with friction”. In: *IEEE Transactions on automatic control* 40.3 (1995), pp. 419–425.

[18] Melvin G Calkin. *Lagrangian and Hamiltonian mechanics*. World Scientific, 1996.

[19] Herbert Goldstein, Charles Poole, and John Safko. *Classical mechanics*. 2002.

[20] Carl Nordling and Jonny Österman. *Physics handbook for science and engineering*. Studentlitteratur ab, 2006.

[21] Steven Kay. “Spectral estimation”. In: *Advanced topics in signal processing* (1988), pp. 58–122.

[22] Katsuhiko Ogata and Yanjuan Yang. *Modern control engineering*. Vol. 5. Prentice hall Upper Saddle River, NJ, 2010.

[23] ISO ISO14791. *Road Vehicles-Heavy Commercial Vehicle Combinations and Articulated Buses-Lateral Stability Test Methods*. Tech. rep. Tech. rep, 2002.

[24] Mitsuji Sampei et al. “Arbitrary path tracking control of articulated vehicles using nonlinear control theory”. In: *IEEE Transactions on Control Systems Technology* 3.1 (1995), pp. 125–131.

[25] A Pedro Aguiar and Joao P Hespanha. “Trajectory-tracking and path-following of underactuated autonomous vehicles with parametric modeling uncertainty”. In: *IEEE transactions on automatic control* 52.8 (2007), pp. 1362–1379.

[26] Hongyan Guo et al. “Dual-envelop-oriented moving horizon path tracking control for fully automated vehicles”. In: *Mechatronics* 50 (2018), pp. 422–433.

[27] JM Park et al. “Obstacle avoidance of autonomous vehicles based on model predictive control”. In: *Proceedings of the Institution of Mechanical Engineers, Part D: Journal of Automobile Engineering* 223.12 (2009), pp. 1499–1516.

[28] Richard S Wallace et al. “First Results in Robot Road-Following.” In: *IJCAI*. Citeseer. 1985, pp. 1089–1095.

[29] Myung-Wook Park, Sang-Woo Lee, and Woo-Yong Han. “Development of lateral control system for autonomous vehicle based on adaptive pure pursuit algorithm”. In: *2014 14th International Conference on Control, Automation and Systems (ICCAS 2014)*. IEEE. 2014, pp. 1443–1447.

[30] Kristoffer Tagesson, Leo Laine, and Bengt Jacobson. “Combining coordination of motion actuators with driver steering interaction”. In: *Traffic injury prevention* 16.sup1 (2015), S18–S24.

[31] *The U.S. Department of Transportation’s Comprehensive Truck Size and Weight Study. Volume I: Summary Report*. 2000. URL: `https://books.google.se/books?id=lx8LLlmXi9oC`.

[32] C MacAdam and M Hagan. “A simple differential brake control algorithm for attenuating rearward amplification in doubles and triples combination vehicles”. In: *Vehicle System Dynamics* 37.sup1 (2002), pp. 234–245.

[33] AMC Odhams et al. “Active steering of a tractor–semi-trailer”. In: *Proceedings of the Institution of Mechanical Engineers, Part D: Journal of Automobile Engineering* 225.7 (2011), pp. 847–869.

[34] Mohammad Manjurul Islam, Leo Laine, and Bengt Jacobson. “Improve safety by optimal steering control of a converter dolly using particle swarm optimization for low-speed maneuvers”. In: *2015 IEEE 18th International Conference on Intelligent Transportation Systems*. IEEE. 2015, pp. 2370–2377.

[35] Sogol Kharrazi. *Steering based lateral performance control of long heavy vehicle combinations*. Chalmers University of Technology, 2012.

[36] Tushita Sikder. “Design of active trailer steering systems for long combination vehicles using robust control techniques”. PhD thesis. 2017.

[37] Laszlo Palkovics, Lajos llosvai, and Akos Semsey. “The self–steering behaviour of a tractor–semi–trailer at high–speed and its control to improve lateral stability”. In: *International Journal of Heavy Vehicle Systems* 1.3 (1994), pp. 304–323.

[38] Jim Karki. “Active low-pass filter design”. In: *Texas Instruments application report* (2000).

[39] George Ellis. *Control system design guide: using your computer to understand and diagnose feedback controllers*. Butterworth-Heinemann, 2012.

[40] Md Manjurul Islam et al. “How well a single-track linear model captures the lateral dynamics of long combination vehicles”. In: *Vehicle system dynamics* 57.12 (2019), pp. 1874–1896.

A

Appendix 1

A.1 Derivation of single-track model for tractor and semitrailer

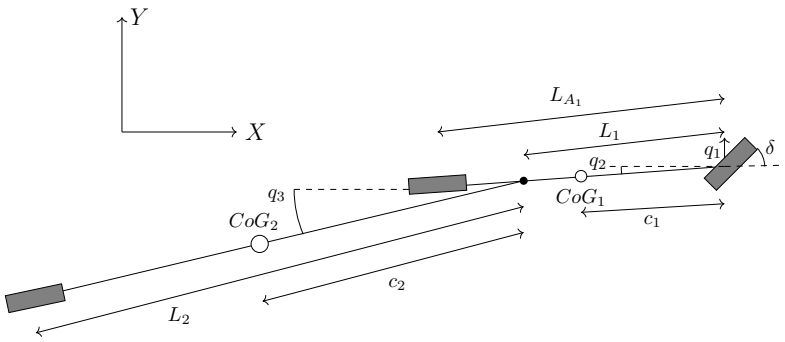

Figure A.1: Bicycle model of tractor and semitrailer.

Parameter	Symbol	Unit
Mass for the tractor	m_1	[kg]
Mass for the trailer	m_2	[kg]
Distance from front wheel to CoG for tractor	c_1	[m]
Distance from articulation point to CoG for trailer	c_2	[m]
Length from front wheels to articulation point	L_{A_1}	[m]
Length from front axle to rear axle	L_1	[m]
Length from articulation point to rear axle of trailer	L_2	[m]
Constant longitudinal velocity	U	[m/s]
Cornering stiffness for wheel i	C_i	[N/°]
Inertia for unit j	I_j	[kgm^2]
Velocity	v	[m/s]
Generalized coordinate j	q_j	

Table A.1: Glossary for the variables used in derivation. Subscripts for the velocities, for example $Gx1$, should be read as: At CoG in x-axis for unit one.

Since planar motion is considered the potential energy V=0. Hence L only contains the kinematic energy. Looking at Figure A.1, the total kinematic energy from the tractor and semitrailer is

$$
\begin{aligned}
T &= \frac{1}{2}m_1(v_{Gx1}^2 + v_{Gy1}^2) + \frac{1}{2}m_2(v_{Gx2}^2 + v_{Gy2}^2) + \frac{1}{2}I_1\dot{q}_2^2 + \frac{1}{2}I_2\dot{q}_3^2 \\
v_{Gx1}^2 &= \Big(U + \dot{q}_2 c_1 \sin(q_2)\Big)^2 \\
v_{Gy1}^2 &= \Big(\dot{q}_1 - \dot{q}_2 c_1 \cos(q_2)\Big)^2 \\
v_{Gx2}^2 &= \Big(\dot{q}_3 c_2 \sin(q_3) + U + \dot{q}_2 L_{A_1} \sin q_2\Big)^2 \\
v_{Gy2}^2 &= \Big(- \dot{q}_3 c_2 \cos q_3 + \dot{q}_1 - \dot{q}_2 L_{A_1} \cos(q_2)\Big)^2
\end{aligned}
\tag{A.1}
$$

Using small angle assumption and only keeping linear terms gives the velocities

$$v_{Gx1}^2 = \Big(U + \dot{q}_2 c_1 \sin(q_2)\Big)^2 \approx U^2 \tag{A.2}$$

$$v_{Gy1}^2 = \Big(\dot{q}_1 - \dot{q}_2 c_1 \cos(q_2)\Big)^2 \approx (\dot{q}_1 - \dot{q}_2 c_1)^2 \tag{A.3}$$

$$v_{Gx2}^2 = \Big(\dot{q}_3 c_2 \sin(q_3) + U + \dot{q}_2 L_{A_1} \sin q_2\Big)^2 \approx U^2 \tag{A.4}$$

$$v_{Gy2}^2 = \Big(- \dot{q}_3 c_2 \cos q_3 + \dot{q}_1 - \dot{q}_2 L_{A_1} \cos(q_2)\Big)^2 \approx (-\dot{q}_3 c_2 + \dot{q}_1 - \dot{q}_2 L_{A_1})^2 \tag{A.5}$$

Calculating the partial derivatives on the left hand side in equation 2.2 gives

$$
\begin{aligned}
\frac{d}{dt}\Big(\frac{\partial v_{Gy1}^2}{\partial \dot{q}_1}\Big) &= 2(\ddot{q}_1 - c_1\ddot{q}_2) \\
\frac{d}{dt}\Big(\frac{\partial v_{Gy2}^2}{\partial \dot{q}_1}\Big) &= 2(\ddot{q}_1 - c_2\ddot{q}_3 - \ddot{q}_2 L_{A_1}) \\
\frac{d}{dt}\Big(\frac{\partial v_{Gy1}^2}{\partial \dot{q}_2}\Big) &= -2c_1(\ddot{q}_1 - c_1\ddot{q}_2) \\
\frac{d}{dt}\Big(\frac{\partial v_{Gy2}^2}{\partial \dot{q}_2}\Big) &= -2L_{A_1}(\ddot{q}_1 - \ddot{q}_2 L_{A_1} - \ddot{q}_3 c_2) \\
\frac{d}{dt}(\frac{\partial v_{Gy2}^2}{\partial \dot{q}_3}) &= -2c_2(\ddot{q}_1 - \ddot{q}_2 L_{A_1} - \ddot{q}_3 c_2) \\
\frac{d}{dt}\Big(\frac{\partial v_{Gx1}^2}{\partial \dot{q}_1}\Big) &= \frac{d}{dt}\Big(\frac{\partial v_{Gx2}^2}{\partial \dot{q}_1}\Big) = \frac{d}{dt}\Big(\frac{\partial v_{Gx1}^2}{\partial \dot{q}_2}\Big) = \frac{d}{dt}\Big(\frac{\partial v_{Gx2}^2}{\partial \dot{q}_2}\Big) = \dots \\
&= \frac{d}{dt}(\frac{\partial v_{Gx1}^2}{\partial \dot{q}_3}) = \frac{d}{dt}(\frac{\partial v_{Gy1}^2}{\partial \dot{q}_3}) = \frac{d}{dt}(\frac{\partial v_{Gx2}^2}{\partial \dot{q}_3}) = 0
\end{aligned}
\tag{A.6}
$$

Moreover, by checking the equations (A.1) one can easily observe that

$$\frac{\partial T}{\partial q_1} = \frac{\partial T}{\partial q_2} = \frac{\partial T}{\partial q_3} = 0. \tag{A.7}$$

Hence when adding (A.6) and (A.7) together with respect to each global coordinate the resulting system the equations become

$$\frac{d}{dt}\Big(\frac{\partial T}{\partial \dot{q}_1}\Big) - \frac{\partial T}{\partial q_1} = \frac{1}{2}m_1\Big(2(\ddot{q}_1 - \ddot{q}_2 c_1)\Big) + \frac{1}{2}m_2\Big(2(-\ddot{q}_3 c_2 + \ddot{q}_1 - \ddot{q}_2 L_{A_1})\Big) \tag{A.8}$$

$$\begin{aligned}\frac{d}{dt}\Big(\frac{\partial T}{\partial \dot{q}_2}\Big) - \frac{\partial T}{\partial q_2} &= \frac{1}{2}m_1\Big(-2c_1(\ddot{q}_1 - c_1\ddot{q}_2)\Big) \\ &\quad + \frac{1}{2}m_2\Big(-2L_{A_1}(\ddot{q}_1 - \ddot{q}_2 L_{A_1} - \ddot{q}_3 c_2)\Big) + 2\frac{1}{2}I_1\ddot{q}_2\end{aligned} \tag{A.9}$$

$$\frac{d}{dt}\Big(\frac{\partial T}{\partial \dot{q}_3}\Big) - \frac{\partial T}{\partial q_3} = \frac{1}{2}m_2\Big(-2c_2(\ddot{q}_1 - \ddot{q}_2 L_{A_1} - \ddot{q}_3 c_2)\Big) + 2\frac{1}{2}I_2\ddot{q}_3 \tag{A.10}$$

$$\tag{A.11}$$

Simplifying the equations yield

$$\frac{d}{dt}\Big(\frac{\partial T}{\partial \dot{q}_1}\Big) - \frac{\partial T}{\partial q_1} = m_1(\ddot{q}_1 - \ddot{q}_2 c_1) + m_2(-\ddot{q}_3 c_2 + \ddot{q}_1 - \ddot{q}_2 L_{A_1}) \tag{A.12}$$

$$\frac{d}{dt}\Big(\frac{\partial T}{\partial \dot{q}_2}\Big) - \frac{\partial T}{\partial q_2} = m_1 c_1(-\ddot{q}_1 + c_1\ddot{q}_2) + m_2 L_{A_1}(-\ddot{q}_1 + \ddot{q}_2 L_{A_1} + \ddot{q}_3 c_2) + I_1\ddot{q}_2 \tag{A.13}$$

$$\frac{d}{dt}\Big(\frac{\partial T}{\partial \dot{q}_3}\Big) - \frac{\partial T}{\partial q_3} = m_2 c_2(-\ddot{q}_1 + \ddot{q}_2 L_{A_1} + \ddot{q}_3 c_2) + I_2\ddot{q}_3 \tag{A.14}$$

Rearranging such that each variable is separated gives

$$\frac{d}{dt}\Big(\frac{\partial T}{\partial \dot{q}_1}\Big) - \frac{\partial T}{\partial q_1} = \ddot{q}_1(m_1 + m_2) + \ddot{q}_2(-c_1 m_1 - m_2 L_{A_1}) + \ddot{q}_3(-c_2 m_2) \tag{A.15}$$

$$\begin{aligned}\frac{d}{dt}\Big(\frac{\partial T}{\partial \dot{q}_2}\Big) - \frac{\partial T}{\partial q_2} &= \ddot{q}_1(-m_1 c_1 - m_2 L_{A_1}) + \ddot{q}_2(m_1 c_1^2 + m_2 L_{A_1}^2 + I_1) \\ &\quad + \ddot{q}_3(m_2 c_2 L_{A_1})\end{aligned} \tag{A.16}$$

$$\frac{d}{dt}\Big(\frac{\partial T}{\partial \dot{q}_3}\Big) - \frac{\partial T}{\partial q_3} = \ddot{q}_1(-m_2 c_2) + \ddot{q}_2(m_2 c_2 L_{A_1}) + \ddot{q}_3(m_2 c_2^2 + I_2) \tag{A.17}$$

$$\tag{A.18}$$

The system of equations is then transformed into matrix form, gives the system becomes

$$\begin{pmatrix} m_1 + m_2 & -c_1 m_1 - m_2 L_{A_1} & -m_2 c_2 \\ -m_1 c_1 - m_2 L_{A_1} & m_1 c_1^2 + m_2 L_{A_2}^2 + I_1 & m_2 c_2 L_{A_1} \\ -m_2 c_2 & m_2 c_2 L_{A_1} & m_2 c_2^2 + I_2 \end{pmatrix} \begin{pmatrix} \ddot{q}_1 \\ \ddot{q}_2 \\ \ddot{q}_3 \end{pmatrix} = \mathbb{Q} \tag{A.19}$$

Now considering the right hand side of the equation. The total power done on the system is

$$P = P_1 + P_2 + P_3$$

where P_1, P_2 and P_3 is the power contributed from each of the wheels where the work on the wheel is calculated as:

$$P_1 = F_1(1,0,0)\begin{pmatrix}\dot{q}_1\\ \dot{q}_2\\ \dot{q}_3\end{pmatrix}; \quad F_1 = C_1\Big(\delta + q_2 - \frac{v_{lat_1}}{U}\Big), \quad v_{lat_1} = \dot{q}_1 \tag{A.20}$$

$$P_2 = F_2(1,-L_1,0)\begin{pmatrix}\dot{q}_1\\ \dot{q}_2\\ \dot{q}_3\end{pmatrix}; \quad F_2 = C_2\Big(q_2 - \frac{v_{lat_2}}{U}\Big), \quad v_{lat_2} = \dot{q}_1 - \dot{q}_2 L_1 \tag{A.21}$$

$$P_3 = F_3(1,-L_{A_1},-L_2)\begin{pmatrix}\dot{q}_1\\ \dot{q}_2\\ \dot{q}_3\end{pmatrix}; \quad F_3 = C_3\Big(q_3 - \frac{v_{lat_3}}{U}\Big), \tag{A.22}$$

$$, v_{lat_3} = \dot{q}_1 - \dot{q}_2 L_{A_1} - \dot{q}_3 L_2$$

Since the power contribution w_1 can be written as

$$P_1 = F_1 \cdot v_1 \tag{A.23}$$

and noticing that the work is a scalar product from a system of equations one can combine it with equation (2.3) to write the work on the following matrix form.

$$P = \mathbb{Q}^T \cdot \vec{\dot{q}} = \begin{pmatrix} F_1 + F_2 + F_3 \\ -L_1 F_2 - L_{A_1} F_3 \\ -L_2 F_3 \end{pmatrix}^T \begin{pmatrix}\dot{q}_1\\ \dot{q}_2\\ \dot{q}_3\end{pmatrix} \tag{A.24}$$

From (2.2) one notice that Q is the corresponds to the right hand side of the equation. Expanding $\mathbb{Q}$ gives

$$\mathbb{Q} = \begin{pmatrix} F_1 + F_2 + F_3 \\ -L_1 F_2 - L_{A_1} F_3 \\ -L_2 F_3 \end{pmatrix} \tag{A.25}$$

$$= \begin{pmatrix} C_1\Big(\delta + q_2 - \dot{q}_1/U\Big) + C_2\Big(q_2 - (\dot{q}_1 - \dot{q}_2 L_1)/U\Big) + C_3\Big(q_3 - (\dot{q}_1 - \dot{q}_2 L_{A_1} - \dot{q}_3 L_2)/U\Big) \\ -L_1 C_2\Big(q_2 - (\dot{q}_1 - \dot{q}_2 L_1)/U\Big) - L_{A_1} C_3\Big(q_3 - (\dot{q}_1 - \dot{q}_2 L_{A_1} - \dot{q}_3 L_2)/U\Big) \\ -L_2 C_3\Big(q_3 - (\dot{q}_1 - \dot{q}_2 L_{A_1} - \dot{q}_3 L_2)/U\Big) \end{pmatrix}$$

Separating the equations into separate matrices gives

$$\mathbb{Q} = \frac{1}{U}\begin{pmatrix} -(C_1 + C_2 + C_3) & C_2 L_1 + C_3 L_{A_1} & C_3 L_2 \\ L_1 C_2 + L_{A_1} C_3 & -L_1^2 C_2 - L_{A_1}^2 C_3 & -L_{A_1} C_3 L_2 \\ L_2 C_3 & -L_{A_1} L_2 C_3 & -L_2^2 C_3 \end{pmatrix}\begin{pmatrix}\dot{q}_1\\ \dot{q}_2\\ \dot{q}_3\end{pmatrix} \tag{A.26}$$

$$+ \begin{pmatrix} 0 & C_1 + C_2 & C_3 \\ 0 & -L_1 C_2 & -L_{A_1} C_3 \\ 0 & 0 & -L_2 C_3 \end{pmatrix}\begin{pmatrix} q_1 \\ q_2 \\ q_3 \end{pmatrix} + \begin{pmatrix} C_1 \delta \\ 0 \\ 0 \end{pmatrix} \tag{A.27}$$

Renaming the matrices gives

$$M = \begin{pmatrix} m_1 + m_2 & -c_1 m_1 - m_2 L_{A_1} & -m_2 c_2 \\ -m_1 c_1 - m_2 L_{A_1} & m_1 c_1^2 + m_2 L_{A_2}^2 + I_1 & m_2 c_2 L_{A_1} \\ -m_2 c_2 & m_2 c_2 L_{A_1} & m_2 c_2^2 + I_2 \end{pmatrix} = \begin{pmatrix} M_1 & M_2 & M_3 \\ M_4 & M_5 & M_6 \\ M_7 & M_8 & M_9 \end{pmatrix} \tag{A.28}$$

$$N = \frac{1}{U} \begin{pmatrix} -(C_1 + C_2 + C_3) & C_2 L_1 + C_3 L_{A_1} & C_3 L_2 \\ L_1 C_2 + L_{A_1} C_3 & -L_1^2 C_2 - L_{A_1}^2 C_3 & -L_{A_1} C_3 L_2 \\ L_2 C_3 & -L_{A_1} L_2 C_3 & -L_2^2 C_3 \end{pmatrix} = \begin{pmatrix} N_1 & N_2 & N_3 \\ N_4 & N_5 & N_6 \\ N_7 & N_8 & N_9 \end{pmatrix} \tag{A.29}$$

$$K = \begin{pmatrix} 0 & C_1 + C_2 & C_3 \\ 0 & -L_1 C_2 & -L_{A_1} C_3 \\ 0 & 0 & -L_2 C_3 \end{pmatrix} = \begin{pmatrix} K_1 & K_2 & K_3 \\ K_4 & K_5 & K_6 \\ K_7 & K_8 & K_9 \end{pmatrix} \tag{A.30}$$

$$\Delta = \begin{pmatrix} C_1 \delta \\ 0 \\ 0 \end{pmatrix} \tag{A.31}$$

By combining the left and right side terms one obtains the ODE-system

$$M\vec{\ddot{q}} - N\vec{\dot{q}} - K\vec{q} - \Delta = \mathbf{0}. \tag{A.32}$$

Rearranging the equation such that $\ddot{q}$ is isolated on the left hand side gives

$$\vec{\ddot{q}} = \underbrace{M^{-1}N}_{H}\vec{\dot{q}} + \underbrace{M^{-1}K}_{W}\vec{q} + \underbrace{M^{-1}\Delta}_{R} = H\vec{\dot{q}} + W\vec{q} + R, \tag{A.33}$$

where $H, W \in \mathbb{R}^{3\times3}$ and $R \in \mathbb{R}^{3\times1}$. Introducing the new state vector x defined as

$$\vec{x} = \begin{pmatrix} x_1 \\ x_2 \\ x_3 \\ x_4 \\ x_5 \\ x_6 \end{pmatrix}, \quad x_i = \begin{cases} q_i, & i = 1, 2, 3 \\ \dot{q}_{i-3}, & i = 4, 5, 6 \end{cases} \tag{A.34}$$

results the simpler linear ODE-system

$$\vec{\dot{x}} = A\vec{x} + B, \tag{A.35}$$

where A and B are composed of

$$A = \begin{pmatrix} 0 & 0 & 0 & 1 & 0 & 0 \\ 0 & 0 & 0 & 0 & 1 & 0 \\ 0 & 0 & 0 & 0 & 0 & 1 \\ W_1 & W_2 & W_3 & H_1 & H_2 & H_3 \\ W_4 & W_5 & W_6 & H_4 & H_5 & H_6 \\ W_7 & W_8 & W_9 & H_7 & H_8 & H_9 \end{pmatrix}, \quad B = \begin{pmatrix} 0 \\ 0 \\ 0 \\ R_1 \\ R_2 \\ R_3 \end{pmatrix}. \tag{A.36}$$

A.2 Resulting rearward amplification from extreme case for different sizes of preview time and number of preview points

PT [ms] /PP	2	3	4	5	6	7	8	9	10	11
100	1.2796	1.2708	1.2775	1.2710	1.2710	1.2713	1.2728	1.2773	1.2780	1.2782
200	1.2889	1.2727	1.2714	1.2725	1.2730	1.2723	1.2634	1.2723	1.2723	1.2715
300	1.2792	1.2633	1.2463	1.2477	1.2451	1.2440	1.2456	1.2448	1.2477	1.2456
400	1.2897	1.2507	1.2489	1.2485	1.2493	1.2483	1.2489	1.2563	1.2692	1.2828
500	1.2353	1.2351	1.2353	1.2351	1.2363	1.2346	1.2345	1.2358	1.2736	1.2736
600	1.2258	1.2246	1.2261	1.2263	1.2258	1.2178	1.2178	1.2178	1.2178	1.2154
700	1.2262	1.1385	1.1510	1.1385	1.1538	1.2718	1.2720	1.2720	1.1525	1.1361
800	1.1355	1.1565	1.1502	1.1663	1.1290	1.1051	1.1290	1.1562	1.1537	1.1537
900	1.2060	1.2347	1.2347	1.2347	1.2378	1.2347	1.2347	1.2352	1.2352	1.2441
1000	1.1763	1.1786	1.1749	1.1755	1.1755	1.1755	1.1707	1.1707	1.2009	1.2009

Table A.2: Rearward amplification generated from different amounts of preview points and size of preview time distance. PP is the abbreviation of preview points and PT the preview time.

PT [ms] /PP	2	3	4	5	6	7	8	9	10	11
100	0.1759	0.1748	0.1758	0.1748	0.1749	0.1749	0.1751	0.1757	0.1759	0.1759
200	0.1765	0.1746	0.1745	0.1745	0.1746	0.1745	0.1734	0.1745	0.1745	0.1744
300	0.1760	0.1737	0.1710	0.1710	0.1709	0.1707	0.1708	0.1708	0.1711	0.1707
400	0.1759	0.1699	0.1698	0.1697	0.1698	0.1697	0.1698	0.1707	0.1717	0.1757
500	0.1683	0.1683	0.1683	0.1683	0.1683	0.1683	0.1682	0.1684	0.1737	0.1737
600	0.1614	0.1615	0.1615	0.1615	0.1614	0.1605	0.1605	0.1605	0.1605	0.1601
700	0.1597	0.1782	0.1725	0.1782	0.1724	0.1665	0.1665	0.1665	0.1794	0.1767
800	0.1885	0.1817	0.1822	0.1824	0.1759	0.1746	0.1759	0.1812	0.1819	0.1819
900	0.1464	0.1511	0.1511	0.1511	0.1515	0.1511	0.1511	0.1511	0.1511	0.1525
1000	0.1548	0.1502	0.1503	0.1502	0.1502	0.1502	0.1503	0.1503	0.1549	0.1549

Table A.3: Maximum absolute yaw-rate in rad/s observed from different amounts of preview points and size of preview time distance. PP is the abbreviation of preview points and PT the preview time.